Internal Report ITeSRE 296/2000

September 2000

THEORETICAL IMPLICATIONS OF FUTURE CMB SPECTRUM OBSERVATIONS

R. Salvaterra and C. Burigana

Istituto TeSRE/CNR, via P. Gobetti 101, I-40129 Bologna, Italy

Internal Report ITeSRE 296/2000

THEORETICAL IMPLICATIONS OF FUTURE CMB SPECTRUM OBSERVATIONS

R. Salvaterra and C. Burigana

Istituto TeSRE/CNR, via P. Gobetti 101, I-40129 Bologna, Italy

SUMMARY – We have studied the implications of possible future observations of the CMB absolute temperature at $\lambda > 1$ cm, where both ground (TRIS), balloon and satellite (DIMES) experiments are currently under study to complement the accurate FIRAS data at $\lambda < 1$ cm.

Our analysis shows that future measures from ground and balloon will not be able to significantly improve the constraints on energy dissipations in the primeval plasma already provided by the FIRAS data. Even observations with a sensitivity better by a factor 10 with respect to the realistic performances of the next experiments at different cm and dm wavelengths can not significantly improve this conclusion.

Thus, we have studied the impact of very high quality data, such those that could be in principle reached with a spacecraft experiment like DIMES, planned to measure the CMB absolute temperature at $0.5 < \lambda < 15$ cm with a sensitivity of $0.02 \div 0.2$ mK, comparable to that of FIRAS (Fixsen et al. 1996, Mather et al. 1999). We have demonstrated that these data would represent a substantial improvement for our knowledge of energy dissipation processes at medium and high redshifts ($y_h \gtrsim 1$): the constraints on $\Delta\epsilon/\epsilon_i$ can be improved by two order of magnitude for processes occurring in a wide range of cosmic epochs.

By the jointed analysis of two dissipation processes occurring at different epochs, we demonstred that with the sensitivity and frequency coverage of a DIMES-like experiment it would be possible to accurately recover the amount of energy possibly injected in the radiation field at early and medium epochs even in presence of a possible late distortion. Also the epoch of energy dissipation could be significantly constrained, whereas only poor informations on the baryon density can be derived.

1 Introduction

As widely discussed in many papers, the spectrum of the Cosmic Microwave Background (CMB) carries unique informations on physical processes occurring during early cosmic epochs (see e.g. Danese & Burigana 1993 and references therein). The comparison between models of CMB spectral distortions and CMB absolute temperature measures can constrain the physical parameters of the considered dissipation processes. Burigana & Salvaterra 2000 discussed the implications of the current CMB spectrum data. We will extend here that analysis by jointly considering the data from the FIRAS instrument aboard the COBE satellite and simulated sets of CMB spectrum observations at wavelenghts larger than 1 cm with the sensitivities expected from future experiments in order to discuss their impact for the recovery of the thermal history of the universe.

1.1 Theoretical framework

The CMB spectrum emerges from the thermalization redshift, $z_{therm} \sim 10^6 \div 10^7$, with a shape very close to a planckian one, owing to the strict coupling between radiation and matter through Compton scattering and photon production/absorption processes, radiative Compton and Bremsstrahlung, which were extremely efficient at early times and able to re-establish a blackbody (BB) spectrum from a perturbed one on timescales much shorter than the expansion time (e.g. Danese & De Zotti 1977). The value of z_{therm} (Burigana et al. 1991a) depends on the baryon density and the Hubble constant through the product $\widehat{\Omega}_b = \Omega_b (H_0/50)^2$ (H_0 expressed in Km/s/Mpc).

Physical processes occurring at redshifts $z < z_{therm}$ may lead an imprinting on the CMB spectrum. The CMB distorted spectra depend on at least three main parameters: the fractional amount of energy exchanged between matter and radiation, $\Delta\epsilon/\epsilon_i$, ϵ_i being the radiation energy density before the energy injection, the redshift z_h at which the heating occurs, and the baryon density Ω_b, in units of the critical density.

The analysis of the constraints on the thermal history of the universe set by the high accuracy measurements that have been recently accumulated requires the use of manageable formulae describing spectral distortions for a wide range of the relevant parameters.

The timescale for the achievement of kinetic equilibrium between radiation and matter (i.e. the relaxation time for the photon spectrum), t_C, is

$$t_C = t_{\gamma e} \frac{mc^2}{kT_e} \simeq 4.5 \times 10^{28} \, (T_0/2.7\,K)^{-1} \, \phi^{-1} \widehat{\Omega}_b^{-1} \, (1+z)^{-4} \, \mathrm{sec}\,, \tag{1}$$

where $t_{\gamma e} = 1/(n_e \sigma_T c)$ is the photon–electron collision time, $\phi = (T_e/T_r)$, T_e being the electron temperature and $T_r = T_0(1+z)$; kT_e/mc^2 is the mean fractional change of photon energy in a scattering of cool photons off hot electrons, i.e. $T_e \gg T_r$; T_0 is the present radiation temperature related to the present radiation energy density by $\epsilon_{r0} = aT_0^4$; a primordial helium abundance of 25% by mass is here assumed.

It is useful to introduce the dimensionless time variable $y_e(z)$ defined by

$$y_e(z) = \int_t^{t_0} \frac{dt}{t_C} = \int_1^{1+z} \frac{d(1+z)}{1+z} \frac{t_{exp}}{t_C}\,, \tag{2}$$

where t_0 is the present time and t_{exp} is the expansion time given by

$$t_{exp} \simeq 6.3{\times}10^{19} \left(\frac{T_0}{2.7\,K}\right)^{-2} (1{+}z)^{-3/2} \left[\kappa(1+z) + (1+z_{eq}) - \left(\frac{\Omega_{nr}-1}{\Omega_{nr}}\right)\left(\frac{1+z_{eq}}{1+z}\right)\right]^{-1/2} \mathrm{sec}\,, \tag{3}$$

$z_{eq} = 1.0 \times 10^4 (T_0/2.7\,K)^{-4} \widehat{\Omega}_{nr}$ being the redshift of equal non relativistic matter and photon energy densities (Ω_{nr} is the density of non relativistic matter in units of critical density); $\kappa = 1 + N_\nu (7/8)(4/11)^{4/3}$, N_ν being the number of relativistic, 2–component, neutrino species (for 3 species of massless neutrinos, $\kappa \simeq 1.68$), takes into account the contribution of relativistic neutrinos to the dynamics of the universe[1].

Burigana et al. 1991b have reported on numerical solutions of the Kompaneets equation (Kompaneets 1956) for a wide range of values of the relevant parameters.

Under the assumptions of *i*) small distortions, *ii*) dissipative processes with negligible photon production, *iii*) heating close to be instantaneous, a good approximation if the timescale for energy dissipation is much smaller than the expansion timescale, *iv*) distorted radiation spectrum initially represented by a superposition of blackbodies, as is the case for a broad variety of situations of cosmological interest, Burigana et al. 1995 found accurate analytical representations of the numerical solutions for the photon occupation number η computed by Burigana et al. 1991b. They can be expressed in the form

$$\eta = \eta(x; \Delta\epsilon/\epsilon_i, y_h, \widehat{\Omega}_b)\,, \tag{4}$$

where x is the dimensionless frequency $x = h\nu/kT_0$ (ν being the present frequency), and $y_h \equiv y_e(z_h)$ characterizes the epoch when the energy dissipation occurred, z_h being the corresponding redshift (we will refer to $y_h \equiv y_e(z_h)$ computed assuming $\phi = 1$, so that the epoch considered for the energy dissipation does not depend on the amount of released energy).

The form of these analytical approximations is in part suggested by the general properties of the Kompaneets equation and by its well known asymptotic solutions. For $y_h \ll 1$ a superposition of blackbodies is, to a very good approximation, a solution of the Kompaneets equation, except at very low frequencies where photon emission processes are important; when they dominate the Kompaneets equation reduces to an ordinary differential equation. The Comptonization distortion produced by hot gas at small z is a typical example of superposition of blackbodies (Zeldovich & Sunyaev 1969; Zeldovich et al. 1972). At the other extreme ($y_h \gtrsim 5$) the solution is well described by a Bose-Einstein (BE) formula with a frequency dependent chemical potential. For intermediate values of y_h, η has a shape somewhere between these two limiting cases. For $y_h < 1$ the shape of the distorted spectra at long wavelengths is characterized by a minimum of the brightness temperature.

Of course, by combining the approximations describing the distorted spectrum at early and intermediate epochs with the Comptonization distortion expression describing late distortions, we are able to treat two heating processes simultaneously.

1.2 Comparison between observations and models

In this report we compare the recent measures of the CMB absolute temperature with the above models of distorted spectra for one or two heating processes by using a standard χ^2 analysis. We use the same approach widely described in Burigana & Salvaterra 2000 (see their Appendix A for the details of the code).

We determine the limits on the amount of energy possibly injected in the cosmic background at arbitrary primordial epochs corresponding to a redshift z_h (or equivalently to y_h). This topic has been discussed in several works (see e.g. Burigana et al. 1991b, Nordberg & Smoot 1998, Burigana & Salvaterra 2000). As in Burigana & Salvaterra 2000, we improve here the previous methods of analysis by investigating the possibility of properly combining

[1] Strictly speaking the present ratio of neutrino to photon energy densities, and hence the value of κ, is itself a function of the amount of energy dissipated. The effect, however, is never very important and is negligible for very small distortions.

FIRAS data with longer wavelength measurements with the sensitivities expected for new spectrum experiments and by refining the method of comparison with the theoretical models. We will consider the recent improvement in the calibration of the FIRAS data, that sets the CMB scale temperature at 2.725 ± 0.002 K at 95% of confidence level (CL) (Mather et al. 1999). We do not consider the effect on the estimate of the amount of energy injected in the CMB at a given epoch introduced by the calibration uncertainty of FIRAS scale temperature when FIRAS data are treated jointly to longer wavelength measures, since the analysis of Burigana & Salvaterra 2000 shows that only minor effects are introduced by changing the FIRAS calibration.

Then, we study the combined effect of two different heating processes that may have distorted the CMB spectrum at different epochs. This hypothesis has been also taken into account by Nordberg & Smoot 1998, who fit the observed data with a spectrum distorted by a single heating at $y_h = 5$, a second one at $y_h \ll 1$ and by free-free emission, obtaining limits on the parameters that describe these processes. As in Burigana & Salvaterra 2000, we extend their analysis by considering the full range of epochs for the early and intermediate energy injection process, by taking advantage of the analytical representation of spectral distortions at intermediate redshifts (Burigana et al. 1995). We neglect the free-free distortions produced in the case of late dissipation processes in this joint analysis of two heating processes, because the relationship between free-free distortion and Comptonization distortion depends on the details of the thermal history at late epochs (Danese & Burigana 1993, Burigana et al. 1995) and can not simply represented by integral parameters. In addition, free-free distortions are particularly important at very long wavelengths, where the measurements have the largest error bars and no significant improvements are expected in the future, at least for energy injection processes which give positive distortion parameters; for cooling processes, which generate negative distortion parameters, the effect may be more relevant also at centimetric wavelengths, but the connection between free-free and Comptonization distortion becames even more critical.

It is also possible to extend the limits on $\Delta\epsilon/\epsilon_i$ for heatings occurred at $z_h > z_1$, where z_1 is the redshift corresponding to $y_h = 5$, when the Compton scattering was able to restore the kinetic equilibrium between matter and radiation on timescales much shorter than the expansion time and the evolution on the CMB spectrum can be easily studied by replacing the full Kompaneets equation with the differential equations for the evolution of the electron temperature and the chemical potential. This study can be performed by using the simple analytical expressions by Burigana et al. 1991b instead of numerical solutions.

A recent analysis of the limits on the amount of the energy possibly injected in the cosmic background from the currently available data is reported in Burigana & Salvaterra 2000. In particular, they found that the measures at $\lambda > 1$ cm do not significantly contribute to these constraints because of their poor sensitivity compared to that of FIRAS. New and more accurate measurements are also needed in this range, which is particular sensitive to early energy injection processes. In fact, the current constraints on $\Delta\epsilon/\epsilon_i$ at $y_h \sim 5$ are a factor ~ 2 less stringent than those at y_h less than ~ 0.1, because of the frequency coverage of FIRAS, which mainly set the current constraints at the all cosmic epochs. Thus, we are interested to investigate the role of future ground, balloon and satellite experiments at $\lambda > 1$ cm jointed to the FIRAS measures at $\lambda < 1$ cm.

We briefly describe the main experiments currently under study to measure the CMB absolute temperature at $\lambda > 1$ cm (see section 2). In particular, we will dwell upon the DIMES satellite experiment (Kogut 1996), submitted to the NASA in 1995, that will measure the CMB absolute temperature at cm wavelengths with a sensitivity of about 0.1 mK.

To evaluate the scientific impact represented by the future experiment improvements, we create different data sets simulating the observation of a not distorted spectrum both from

ground and balloon experiments and from a satellite experiment like DIMES (see section 3.1 and section 4.1 respectively) through the method described in section 2.3. For a DIMES-like experiment, we also explore the possibility of the observation of distorted spectra for different amounts of the energy injected in the radiation field and for different cosmic epochs.

Each data set will be then compared to models of distorted spectra by using the program MINPUZZLE (see Appendix A of Burigana & Salvaterra 2000), to recover the value of $\Delta\epsilon/\epsilon_i$ or constraints on it, the heating epoch, y_h, and the baryon density Ω_b. The results for the simulated data in the case of experiments from ground and balloon in the case of a DIMES-like experiment are given in section 3 and 4, respectively. We include in the text the figures necessary to discuss the main results. All the other relevant plots (Fig.s 23 – 44) are reported in Appendix A.

In a few interesting cases, we extend the results based on the simulated observations from a DIMES-like experiment to dissipation processes at $z_1 \leq z_h < z_{therm}$ in order to analyze the impact of such high quality data also in the case of energy injections at very high redshifts (section 4.5).

For simplicity, we restrict our analysis to the case of a baryon density $\Omega_b = 0.05$, but the method can be simply applied to different values of Ω_b. In principle, $\widehat{\Omega}_b$ could be constrained by CMB spectrum observations in presence of an early distortion, from the wavelength of the minimum of the CMB absolute temperature; in this case, a significant change in the χ^2/DOF value for the different choices of this parameter could indicate a favourite value for $\widehat{\Omega}_b$. For completeness, we discuss in section 5 the frequency coverage and the sensitivity requirements of a long wavelength experiment able to provide a robust baryon density estimation.

Finally, we draw our main conclusions in section 6.

2 Future experiments

The CMB spectrum experiments currently under study are dedicated to improve our knowledge at wavelengths longer than those covered by FIRAS. At cm and dm wavelengths, the available measures typically show large error bars although some experiments are rather accurate (i.e., the measure of Staggs et al. 1996 at $\simeq$ 1 cm). Very accurate data at long wavelengths could give a significant improvement to our knowledge of physical processes in the primeval plasma, particularly at high redshifts.

The projects on study regard measurements both from ground and from satellite. We refer here to the project of the ground experiment TRIS at very long wavelengths and to the DIMES experiment from spacecraft (Kogut 1996) that would give very accurate measures in the range 0.5 - 15 cm.

2.1 TRIS

TRIS[2] is a set of total power radiometers designed to measure the absolute temperature of the CMB at three frequencies: 600, 820 and 2500 MHz (50, 36.6 and 12 cm).

In this frequency range the measurements are difficult because the CMB signal is comparable to other components of the antenna temperature: galactic background, unresolved extra-galactic sources, sidelobes pickup and atmospheric emission. To improve the experimental situation, TRIS will make absolute maps of large areas of the sky at the three frequencies, to disentangle the various components of the celestial signal; all the lossy parts of the antenna front ends of the receivers will be cooled down liquid helium temperature, to reduce the thermal noise of these components; the receiver temperatures will be very carefully stabilized to reduce drifts and gain variations.

[2]http://sunradio.uni.mi.astro.it/grupporadio/tris/index.html

The TRIS expected sensitivity is of about 200 mK at the three frequencies.

2.2 DIMES

DIMES[3] (Diffuse Microwave Emission Survey) is a space mission submitted to the NASA in 1995, that would measure very accurately the CMB spectrum at wavelengths in the range $0.5 \div 15$ cm (Kogut 1996).

DIMES will compare the spectrum of each 10 degree pixel on the sky to a precisely known blackbody to precision of $\simeq 0.1$ mK. The set of receivers is given from six cryogenic radiometers operating in the frequency range $2 \div 100$ GHz with a single external blackbody calibration target common to all channels. The channels have their center frequencies at 2, 4, 6, 10 e 90 GHz respectively. In each channel, a cryogenic radiometer switched for gain stability between an internal reference load and an antenna with 10 degree beam width, will measure the signal change as the antenna alternately views the sky and an external blackbody calibration target. The target temperature will be adjusted to match the sky signal in the lowest frequency band, allowing the absolute temperature to be read off from the target thermometry with minimal corrections for the instrumental signature. With its temperature held constant, the target will rapidly move over the higher-frequencies antenna apertures, effectively comparing the spectrum of diffuse emission from the sky to a precise blackbody. By comparing each channel to the same target, uncertainties in the target emission cancel so that deviations from a blackbody spectral shape may be determined much more precisely than the absolute temperature.

DIMES will compare the spectrum of each 10 degree pixel on the sky to a precisely known blackbody to precision 0.1 mK. This represents a sensitivity improvement by a factor better than 300 with respect to previous measurements at cm wavelengths. The DIMES design is driven by the need to reduce or eliminate systematic errors from instrumental artifacts. The instrument emission will be cooled to 2.7 K, whereas the calibration uncertainty will be minimized by using a single calibration target, common to all channels. The atmospheric emission will be observed from low Earth orbit and the multiple channels measurements will minimize the foreground emission problems.

2.3 Generation of simulated data sets

We collect different data sets, simulating measurements of different CMB spectra, distorted or not, at the frequency ranges of the considered experiments. We add to these simulated data the FIRAS data at higher frequencies according to the most recent calibration at 2.725 K (Mather et al. 1999).

To calculate the theoretical temperature of the CMB spectrum at the wavelengths of the new experiments, we use the program PUZZLE (see Appendix A in Burigana & Salvaterra 2000) for the cases of distorted spectra, whereas the thermodynamic temperature held obviously constant at all the frequencies for the case of a non distorted spectrum. The theoretical temperatures are then fouled to simulate real measurements affected by instrumental noise. The observed temperature T_{obs} at the frequency ν is given by

$$T_{obs}(\nu) = T_{teor}(\nu) + n(\nu) \times \mathrm{err}(\nu),$$

where $T_{teor}(\nu)$ is the theoretical temperature at the frequency ν and $\mathrm{err}(\nu)$ is the expected rms error (at 1 σ) of the experiment at this frequency. The numbers n are a set of random numbers generated according to a Gaussian distribution with null mean value and unit variance with the routine GASDEV by Press et al. 1992 (§7).

[3] http://map.gsfc.nasa.gov/DIMES/index.html

3 Implications of future ground and balloon experiments

3.1 Simulated data sets

We analyse here the impact of possible future observations from ground and balloon in the case of a not distorted spectrum at the temperature $T_0 = 2.725$ K. The results are thus comparable to those obtained with the FIRAS data alone (Burigana & Salvaterra 2000).

To build the first simulated data set, we split the region from 1 to 80 cm in three ranges and associate different values of sensitivity to each range according to the analysis of the main problems affecting the available observations in different spectral regions (e.g. Salvaterra & Burigana 2000).

1. $1 \div 4$ cm. In this range the measurements of Staggs et al. 1996 show an uncertainty of ~ 0.04 K. Thus, quite accurate measures are possible in this range. We choose to associate to the future experiments at these wavelengths an improved typical sensitivity of 0.01 K.

2. $4 \div 9$ cm. Ground experiments in this range show error bars of about $0.05 \div 0.07$ K. Progresses could be reached by improving the accuracy of the subtraction of the atmospheric contribution which dominates the final error at these wavelengths. Thus, we choose to associate to the data in this region a typical sensitivity of 0.04 K;

3. $10 \div 80$ cm. Observations in this range are still quite difficult, the typical sensitivites being between 0.2 K for measures at 10 cm and 1.5 K for those at longer wavelengths. The expected sensitivity of the TRIS experiment (section 2.1) is of ~ 0.2 K. Thus, we choose to associate to future experiments in this range a typical sensitivity of 0.2 K.

We choose the frequencies of the simulated observations by adopting those of the recent experiments at $\lambda > 1$ cm, so avoiding the problems of absence of observation window or of presence of man made interferences that may be present at other frequencies.

Finally, we complete this data set by adding the FIRAS measures calibrated at 2.725 K to the above simulated data.

A second data set is built as before but by improving by a factor 10 the sensitivity associated to each of the above three frequency range in order to evaluate the impact of extremely optimistic future progresses of ground and ballon experiments.

These two data sets are shown in the top and middle panels of Fig. 1.

3.2 Fits to simulated data

The results of the fits to the first and second set of simulated data from ground and balloon jointed to FIRAS data are shown respectively in Fig.s 3 and 4 and in Fig.s 5 and 6.

It is evident that realistic improvements of future experiments from ground and balloon do not significantly change the FIRAS limits.

Even under much more optimistic experimental conditions, able to decrease the errors by a factor 10, the situation can not substantially improve, being the limits on $\Delta\epsilon/\epsilon_i$ obtained in this case only just more stringent than those based on FIRAS data alone.

We then conclude that, unfortunately, observations of the CMB absolute temperature with sensitivity levels typical of future ground and balloon experiments do not seem able to improve the limits on the amount of energy injected in the cosmic radiation field inferred on the basis of the currently available measures.

4 Implications of a DIMES-like experiment

4.1 Simulated data sets

We generate a first set of simulated data in the case of a blackbody spectrum at a temperature of 2.725 K (see bottom panel of Fig. 1) in order to evaluate the capability of an experiment with a sensitivity comparable to that expect for DIMES to improve the constraints on the amount of the energy injected in the cosmic radiation field. The analysis of this case is in fact directly comparable with the results obtained from the fit to the FIRAS data alone.

Then, we build up other data sets representing the observations of CMB spectra distorted by energy injections at different cosmic epochs in order to investigate the possibility of a DIMES-like experiments to firmly determine the presence of spectral distortions. We consider processes occurring at a wide range of cosmic epochs, represented by the dimensionless time $y_h = 5, 4, 3, 2, 1, 0.5, 0.25, 0.1, 0.05, 0.025, 0.01$, and $y_h \ll 1$. We consider four representative values of fractional injected energy, $\Delta\epsilon/\epsilon_i = 2 \times 10^{-5}$ (see Fig. 2), a value not much below the upper FIRAS limits, 2×10^{-4}, well above FIRAS upper limit, and finally 5×10^{-6} and 2×10^{-6}, two values well below the FIRAS upper limit, to test the chances of an experiment like DIMES of detecting very small distortions.

As a further representative case, we simulate also the observation of a spectrum distorted by two heating processes, the first at $y_h = 5$ and the second at $y_h \ll 1$ both characterized by $\Delta\epsilon/\epsilon_i = 5 \times 10^{-6}$.

These distorted spectra are computed by setting $\Omega_b = 0.05$ and $H_0 = 50$ Km/s/Mpc.

As a variance with respect the previous section, we choose here the frequencies of the simulated observations by adopting the five channels of the DIMES experiment.

As in previous section, we complete these data set by adding the FIRAS measures calibrated at 2.725 K.

4.2 Fits to simulated data: non distorted spectra

We fit the blackbody simulated data with a spectrum distorted by an energy injection at different values of y_h in order to recover the value of $\Delta\epsilon/\epsilon_i$, expected to be null, and the limits on it. The fit results are given in Fig.s 7 and 8.

It is evident how future data at this sensitivity level allow a strong improvement of the limits obtained with the FIRAS data alone (for comparison see, e.g., Burigana & Salvaterra 2000). The recovered best-fit value of $\Delta\epsilon/\epsilon_i$ is always compatible with the absence of distortions within the limits at 95% CL. For heating processes at low z ($y_h = 0.1 - 0.01$) the fit is substantially dominated by the FIRAS data and the lower and the upper limits on $\Delta\epsilon/\epsilon_i$ are still $\sim 2 \times 10^{-5}$. On the contrary, for early distortions ($y_h \gtrsim 1$) the low frequency measures of a DIMES-like experiment will allow to improve the FIRAS constraints by a factor $\sim 10 - 50$, the proper value increasing with the considered dissipation redshift. We conclude that measures from an instrument like DIMES could represent a good complement to the FIRAS data.

In the next sections we will analyse in detail the capability of a DIMES-like experiment to determine the presence of spectral distortions possibly present in the CMB spectrum.

4.3 Fits to simulated data: spectra distorted by a single dissipation process

The test reported in the previous section suggests that even small distortions could be determined provided that the dissipation would have occurred at relatively early epochs, $y_h \gtrsim 1$. Thus, we analyse the sensitivity of a DIMES-like experiment in the recovery of the amount

of energy possibly injected in the radiation field and explore also the possibility to determine the dissipation process epoch.

Firstly, we fit the data simulated as above under the hypothesis that the heating epoch is known; more explicitely, we fit the data with a theoretical spectrum distorted by a process occurring at the considered y_h by allowing to optimize $\Delta\epsilon/\epsilon_i$ (and T_0) but by taking y_h fixed. In this way we can see how accurately $\Delta\epsilon/\epsilon_i$ could be in principle recovered.

On the other hand, unless we want to use the CMB spectrum data to constrain theoretical models with a well defined dissipation epoch, we are typically interested to set constraints on the value of $\Delta\epsilon/\epsilon_i$ possibly injected at a given unknown epoch occurring within a relatively wide cosmic period; in addition, many classes of physical processes in the plasma epoch present time parameters to be possibly constrained by the comparison with CMB spectrum observations.

Thus, we focus on the cases of spectra distorted at high ($y_h = 5$), medium ($y_h = 1.5$) and at low ($y_h \ll 1$) redshifts by fitting the simulated data by relaxing the a priori knowledge of the dissipation epoch. In this way we would be able to evaluate the possibility of determining also the epoch of the heating [4] without a priori informations by jointly evaluating the impact of the unknowledge of the dissipation epoch on the recovery of injected energy. We want test also the possibility of deriving at the same time informations on the baryon density.

4.3.1 Energy injections at FIRAS limits – Dissipation epoch: known

We consider the case of the observation of a spectrum distorted at different values of y_h by an energy injection with $\Delta\epsilon/\epsilon_i = 2 \times 10^{-5}$. This value is below, but not much, the FIRAS limit.

The above simulated data are then compared with the theoretical CMB spectrum distorted exactly at y_h by performing the fit over $\Delta\epsilon/\epsilon_i$ and T_0.

Fig.s 9 and 10 show the value of $\Delta\epsilon/\epsilon_i$ found for the different values of y_h and the corresponding χ^2/DOF. For high redshifts ($y_h = 2-5$), $\Delta\epsilon/\epsilon_i$ is precisely determined, whereas for distortions at low z we obtain limits similar to those given from the currently available data. This plot represents an optimistic case, being when considered known the dissipation heating epoch.

4.3.2 Energy injections at FIRAS limits – Dissipation epoch: unknown

Fig.s 11 and 12 show the fit to the data simulated with a spectrum distorted at $y_h = 5$ with $\Delta\epsilon/\epsilon_i = 2 \times 10^{-5}$, compared with CMB theoretical spectra distorted at different values of y_h. Note how the best-fit for $y_h = 5$ gives $\Delta\epsilon/\epsilon_i$ very close to the value used to generated the data set and the limits at 95% CL are very stringent. For lower y_h, the best-fit is far from the input value and the χ^2 increases. Thus, we search for a favourite value of y_h. We obtain that the best-fit is exactly 5.0, the value used to create the data, and the χ^2 increases of 4 when y_h decreases below 2.3834. The dissipation epoch is then determined in the range $5 \div 2.4$ at 95% CL.

By searching also for a favourite value of Ω_b (set to 0.05 in the simulation of the data), we obtain a 68% CL range of $0.01 - 0.096$.

The same analysis carried out in the case of a spectrum distorted at $y_h = 1.5$ with $\Delta\epsilon/\epsilon_i = 2 \times 10^{-5}$ is shown in Fig.s 23 and 24. Also in this case, the recovered value of $\Delta\epsilon/\epsilon_i$ is close to the input one for fits with $y_h \simeq 1.5$ and we are also able to determine a significative range of favourite values of y_h, although wider than in the previous case.

[4] Of course, any energy injection occurred at a certain $y_h > 5$ with a proper higher value of $\Delta\epsilon/\epsilon_i$ would give a distorted spectrum essentially indistinguishable by that generated in the case of a dissipation at $y_h = 5$ with a lower value of $\Delta\epsilon/\epsilon_i$, see section 4.5.

Ω_b is found to be in the range $0.024 - 0.091$ at 68% CL.

These informations on y_h and Ω_b can not be obtained from the fit to the data simulating the observation of a spectrum distorted at $y_h = 0.01$. In fact, in this case the FIRAS data dominate the fit. The fit result is compatible also with energy injections with smaller values of $\Delta\epsilon/\epsilon_i$ at higher z (Fig. 25) and with a non distorted spectrum. The χ^2 value (Fig. 26) does not significantly change when y_h varies.

4.3.3 Energy injections below FIRAS limits – Dissipation epoch: known

A DIMES-like experiment should be able to detect also small spectral distortions. Let consider here tha case of a spectrum distorted from an energy injection with $\Delta\epsilon/\epsilon_i = 5 \times 10^{-6}$, about a factor 10 below the FIRAS limits at 95% CL.

If the the dissipation epoch is known, we find (Fig.s 27 and 28) that for processes at high and medium redshifts the best-fit result is close to the input value of the simulated data, although the limits on $\Delta\epsilon/\epsilon_i$ are not so stringent as in the case with a larger energy injection. For $y_h \gtrsim 1$, a spectral distortion would be firmly detected at 95% CL.

4.3.4 Energy injections below FIRAS limits – Dissipation epoch: unknown

From Fig.s 29 and 30 clearly results that even for small distortions with $\Delta\epsilon/\epsilon_i = 5 \times 10^{-6}$, i.e. well below the FIRAS limits, an experiment like DIMES would provide significative constraints on the dissipation epoch in the case of processes occurring at $y_h \sim 5$. The χ^2 increases of 4 when y_h becomes less that unit and dissipations at low redshifts are clearly excluded. It would be also possible to provide a range of baryon density values, $\Omega_b = 0.01 - 0.18$ at 68% CL.

For a process at $y_h = 1.5$ (Fig.s 31 and 32) it is still possible to determine the amount of injected energy, but the recovered range of epochs is wide, since the χ^2 does not particularly increase with z. Medium redshifts are still compatible and only injections at $y_h \lesssim 0.1$ are excluded at 95% CL.

No significant informations can be obtained from this analysis for processes at $y_h = 0.01$ (Fig.s 33 and 34), as already seen for larger distortions, because of the relevance of FIRAS data with respect to low frequency measures.

4.3.5 Very small energy injections

We made also an attempt of observing distortions due to of We consider also the possibility of detecting very small energy injections, namely with $\Delta\epsilon/\epsilon_i = 2 \times 10^{-6}$.

If the dissipation epoch is known, the result of the fit (Fig.s 35 and 36) shows that for dissipations at high redshifts is also possible to determine a no null distortion. The Fig.s 37 and 38 show that also the dissipation epoch can be rather accurately determined provided that it occurs at $y_h \sim 5$, the χ^2 increasing of 4 when y_h becomes less than 0.5. For energy injections at epochs close to $y_h = 5$ the recovered value of $\Delta\epsilon/\epsilon_i$ is close to the input one. No relevant informations on Ω_b can be obtained.

For dissipations at $y_h \sim 1.5$ (Fig.s 39 and 40) a significative distortion can be also determined, but no significative informations on the dissipation epoch can be derived.

In the case of processes at low z, the (FIRAS dominated) fit (Fig.s 41 and 42) is compatible with an unperturbed spectrum.

4.3.6 Energy injections above FIRAS limits – Dissipation epoch: known

For sake of completeness, we consider the simulated data in the case of the observation of a spectrum distorted at different y_h with $\Delta\epsilon/\epsilon_i = 2 \times 10^{-4}$, a large value that does not seem compatible with the limits derived on the basis of FIRAS data as revised by Fixsen et al. 1996 and Mather et al. 1999, used in this work, although a recent analysis of FIRAS calibration by Battistelli et al. 2000 indicates a possible relaxation by a factor $\simeq 2$ ($\simeq 4$) of the constraints on $\Delta\epsilon/\epsilon_i$ for late (early) processes.

The fits (Fig.s 43 and 44) carried out by assuming to know the dissipation epoch show that the simulated at low frequencies and the FIRAS data at high frequencies are not compatible, since the large χ^2 values.

A possible observational scenario with relatively large low frequency spectral distortions and a spectrum essentially unperturbed at the FIRAS frequencies can not be well explained by the class of distorted spectra considered here. In this case, CMB distorted spectra such those generated in some exotic model (for example radiative decays of massive particles, see, e.g., Silk & Stebbins 1983, Danese & Burigana 1993) with a proper fine tuning of key parameters should be carefully considered.

4.4 Fits to simulated data: joint analysis of two dissipation processes

To complete the analysis of the impact of a possible DIMES-like experiment, we consider the simulated observation of a spectrum distorted by a first energy dissipation at $y_h = 5$ with $\Delta\epsilon/\epsilon_i = 5 \times 10^{-6}$ and a second one at $y_h \ll 1$ with $\Delta\epsilon/\epsilon_i = 5 \times 10^{-6}$. The data are then compared to theoretical spectra distorted by a process at $y_h \ll 1$ and another at any given y_h (y_h =5, 4, 3, 2, 1, 0.5, 0.25, 0.1, 0.05, 0.025 and 0.1 respectively). In Fig.s 13 – 15 we show the results of this analysis. Fig. 13 shows the plot of the limits on the energy injected in the CMB spectrum at a given value of y_h by allowing for a second heating possibly occurred at $y_h \ll 1$; Fig. 14 shows the constraints on the energy injected at low z by allowing for a previous distortion occurred at any given y_h; Fig. 15 shows the χ^2/DOF of the best fit model.

A DIMES-like experiment would allow to firmly determine the presence of the distortion at high z; in particular, at $y_h = 5$ the recovered $\Delta\epsilon/\epsilon_i$ is very close to the input one. On the contrary, for a dissipation at $y_h \ll 1$ the fit is compatible with an unperturbed spectrum, since the FIRAS data dominate the limits on the distortions at low redshifts. The limits on $\Delta\epsilon/\epsilon_i$ for processes at low redshifts are, however, lower by a factor 2 than those obtained with the currently available data.

We find that the χ^2 significantly increases when $y_h < 2$: even in the case of two dissipation processes a DIMES-like experiment would be able to identify a favourite range for the epoch of the energy injection at high z.

4.5 Constraints on very high redshift processes

We extend here at $z_h > z_1$ (i.e. $y_h > 5$) the constraints on $\Delta\epsilon/\epsilon_i$ that would be possible to derive at $z_h = z_1$ ($y_h = 5$) with a DIMES-like experiment. We remember that at $z > z_1$ the Compton scattering and photon production processes is able to restore, after an energy injection, the kinetic equilibrium between matter and radiation, yielding a Bose-Einstein spectrum, and the combined effect of Compton scattering and photon production processes tends to reduce the magnitude of spectral distortions, possibly leading to a blackbody spectrum.

We firstly consider here the case of the simulated observation of a not distorted spectrum, that represents a good test of the possible improvements of an instrument like DIMES, because the limits on $\Delta\epsilon/\epsilon_i$ at relevant redshifts can be directly compared to those obtained with FIRAS data alone. For simplicity, we consider the case of a single energy injection

possibly occurred in the cosmic thermal history. The comparison is shown in Fig. 16. As evident, the constraints on $\Delta\epsilon/\epsilon_i$ can be improved by two order of magnitude for processes possibly occurring in a wide range of cosmic epochs, corresponding to about a decade in redshift at z about 10^6. Of course, large energy injections are still possible at very early epochs close to the thermalization redshift, when primordial nucleosynthesis set the ultimately constraints on energy injections in the cosmic radiation field. For late dissipations, FIRAS data mainly constrain $\Delta\epsilon/\epsilon_i$.

As further examples, we show in Fig.s 17 and 18 the constraints on the energy injections at $z_h \geq z_1$ (together with those for dissipation processes at $z_h < z_1$) in the case of a fit with a single energy injection to simulated observations of a spectrum distorted at $y_h = 5$, respectively with $\Delta\epsilon/\epsilon_i = 2 \times 10^{-5}$ and 5×10^{-6}. The costraints on the thermal history of the universe would be in this case completely different from those shown in Fig. 16. A firm detection of early energy injections would be clearly possible with the considered experimental performances and the constraints on the energy possibly injected at $z > z_1$ could be directly derived from the comparison with such kind of future CMB spectrum data by using simple accurate analytical approximations (Burigana et al. 1991b), as in the present results, or precise numerical solutions (Burigana et al. 1991a).

5 Experimental requirements for a baryon density evaluation

For distortions at relatively high redshifts ($y_h \gtrsim 1$), the value of $\widehat{\Omega}_b$ can be simply determined by the knowledge of the frequency position of the minimum of the CMB absolute temperature:

$$\lambda_{m,BE} \simeq 41.56 \left(\frac{\widehat{\Omega}_b}{0.05}\right)^{-2/3} \mathrm{cm}\,. \tag{5}$$

This opportunity is very powerful in principle, since the dependence of $\lambda_{m,BE}$ on $\widehat{\Omega}_b$ is determined only by the well known physics of the radiation processes in an expanding universe during the radiation dominated era.

In Fig. 19 we report $\lambda_{m,BE}$ as function of $\widehat{\Omega}_b$.

For dissipations at $y_h \gtrsim 5$, the amplitude of this temperature decrement is

$$\Delta T_m \simeq 1.17 \times 10^{-3} \left(\frac{\mu_0}{10^{-5}}\right) \left(\frac{T_0}{2.725\,\mathrm{K}}\right) \left(\frac{\widehat{\Omega}_b}{0.05}\right)^{-2/3} \mathrm{K}\,. \tag{6}$$

Fig.s 20 – 22 show the dependence of ΔT_m on $\widehat{\Omega}_b$ and μ_0.

Eq. (5) gives the range of wavelengths to observe for a firm evaluation of $\widehat{\Omega}_b$. As example, for $\widehat{\Omega}_b = 0.05$ we need to accurately measure the CMB absolute temperature up to wavelengths of about 50 cm, clearly out from the DIMES range. Ground and ballon experiments are currently planned to reach these wavelengths. Moreover, from Eq. (6) the amplitude of the maximum dip of the brightness temperature for the energy dissipations at $y_h > 5$ turns to be at the mK level for $\widehat{\Omega}_b \sim 0.05$ and distortions within FIRAS limits; Burigana et al. 1991a shown that it is about 3 times smaller for energy injections at $y_h \simeq 1$. Experiments designed to estimate $\widehat{\Omega}_b$ through the measure of $\lambda_{m,BE}$ should have a sensitivity level better than ~ 1 mK.

For sake of illustration, we consider the simulated observation of a spectrum distorted at $y_h = 5$ with $\Delta\epsilon/\epsilon_i = 2 \times 10^{-5}$ in a $\widehat{\Omega}_b = 0.05$ universe through a very precise experiment extended up to $\lambda \sim 70$ cm. More precisely, we add to the DIMES channels the cm and dm channels at 0.408, 0.610, 0.820, 1.410, 2.5 and 4.75 GHz (73.5, 49.1, 36.6, 21.3, 12 and 6.3 cm) proposed for the space experiment LOBO dedicated to measure the CMB spectrum at very

low frequencies (Sironi et al. 1995, Pagana & Villa 1996), but we assume a much better sensitivity, comparable to that of the DIMES experiment ($\simeq 0.1$ mK). Again, we generate the simulated data as described in section 2.3. The fit to these simulated data by assuming to know the dissipation epoch shows that it would be possible to accurately determine both the amount of injected energy and the baryon density. We recover $\Delta\epsilon/\epsilon_i = 1.99 \pm 0.09 \times 10^{-5}$ and $\widehat{\Omega}_b = 0.048 \pm 0.003$ (errors at 95% CL).

Unfortunately, experiments at dm wavelengths with a sensitivity better than ~ 1 mK, although very informative in principle, seem to be very far from the current capabilities.

6 Conclusions

We have studied the implications of possible future observations of the CMB absolute temperature at $\lambda > 1$ cm, where both ground (TRIS), balloon and satellite (DIMES) experiments are currently under study to complement the accurate FIRAS data at $\lambda < 1$ cm.

Our analysis shows that future measures from ground and balloon will not be able to significantly improve the constraints on energy dissipations in the primeval plasma already provided by the FIRAS data. Even observations with a sensitivity better by a factor 10 with respect to the realistic performances of the next experiments at different cm and dm wavelengths can not significantly improve this conclusion.

Thus, we have studied the impact of very high quality data, such those that could be in principle reached with a spacecraft experiment. For this analysis, we referred to the DIMES experiment (Kogut 1996), submitted to the NASA in 1995, planned to measure the CMB absolute temperature at $0.5 < \lambda < 15$ cm with a sensitivity of $0.02 \div 0.2$ mK, comparable to that of FIRAS.

We have demonstrated that these data would represent a substantial improvement for our knowledge of energy dissipation processes at medium and high redshifts ($y_h \gtrsim 1$).

Dissipation processes at $y_h = 5$ could be firmly detected even for very small amounts of the injected energy ($\Delta\epsilon/\epsilon_i \sim 2 \times 10^{-6}$). For these early dissipations it would be possible to estimate also the energy injection epoch. Distortions at medium redshifts ($y_h \sim 1.5$) could be also firmly detected although for energy injections, $\Delta\epsilon/\epsilon_i$, larger than about 5×10^{-6}; also in this case interesting information on the heating epoch can be derived.

On the contrary, for late processes ($y_h \lesssim 0.1$) a such kind of experiment can not substantially improve the limits based on the sub-cm FIRAS data, which would still set the constraints on $\Delta\epsilon/\epsilon_i$ at these late epochs.

Possible spectral distortions at $\lambda > 1$ cm compatible with relatively large energy injections, compared to the FIRAS limits, can not be consistently reconciled with the FIRAS data, at least for the class of distortion considered here. In this observational scenario, "exotic" models for spectral distortions should be carefully considered.

By the jointed analysis of two dissipation processes occurring at different epochs, we demonstred that with the sensitivity and frequency coverage of a DIMES-like experiment it would be possible to accurately recover the amount of energy possibly injected in the radiation field at early and medium epochs even in presence of a possible late distortion.

In general, the constraints on $\Delta\epsilon/\epsilon_i$ can be improved by two order of magnitude for processes possibly occurring in a wide range of cosmic epochs, corresponding to about a decade in redshift at z about 10^6.

Of course, large energy injections at very early epochs, precedent or close to the thermalization redshift z_{therm}, can not be constrained by CMB spectrum observations; at these early stages primordial nucleosynthesis analysis play the crucial role.

A firm detection of early energy injections would be clearly possible with these experimen-

tal performances and the constraints on the energy possibly injected at $z_{therm} > z > z_1 \simeq 5$ could be directly derived from the comparison with such kind of future CMB spectrum data by using simple accurate analytical approximations (Burigana et al. 1991b), as in the present results, or precise numerical solutions (Burigana et al. 1991a).

Finally, only quite poor contraints on the baryon density can be set by experiments that, although very precise, do not have the necessary frequency coverage at dm wavelenghts. Experiments currently planned at wavelenghts $\gtrsim 20$ cm do not present the high sensitivity ($\sim$ mK) necessary to reach this goal.

Acknowledgements. It is a pleasure to thank M. Bersanelli, L. Danese, G. De Zotti, N. Mandolesi, G. Palumbo and G. Sironi for useful and stimulating discussions.

Figure 1: Simulated data sets in the case of future observations of a not distorted spectrum at 2.725 K. The plots refer respectively to future ground and balloon observations with realistic sensitivities (top panel), to future ground and balloon observations with sensitivities 10 times better (middle panel) and the the sensitivity reachable with an experiment with a sensitivity like that of DIMES (bottom panel).

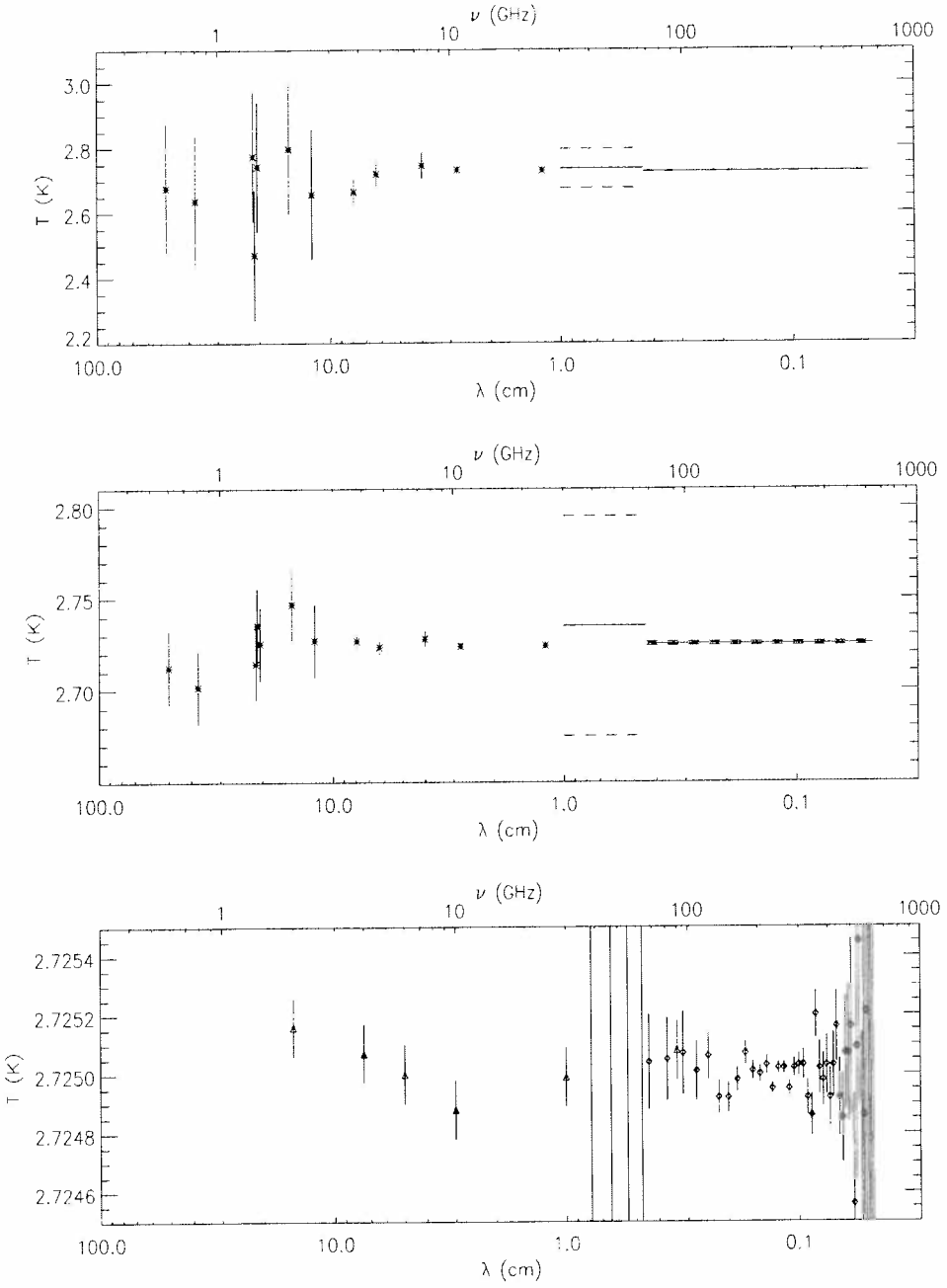

Figure 2: Simulated data sets in the case of the observation of a spectrum distorted at $y_h = 5$ with $\Delta\epsilon/\epsilon_i = 2 \times 10^{-5}$ performed with an instrument with the DIMES sensivity.

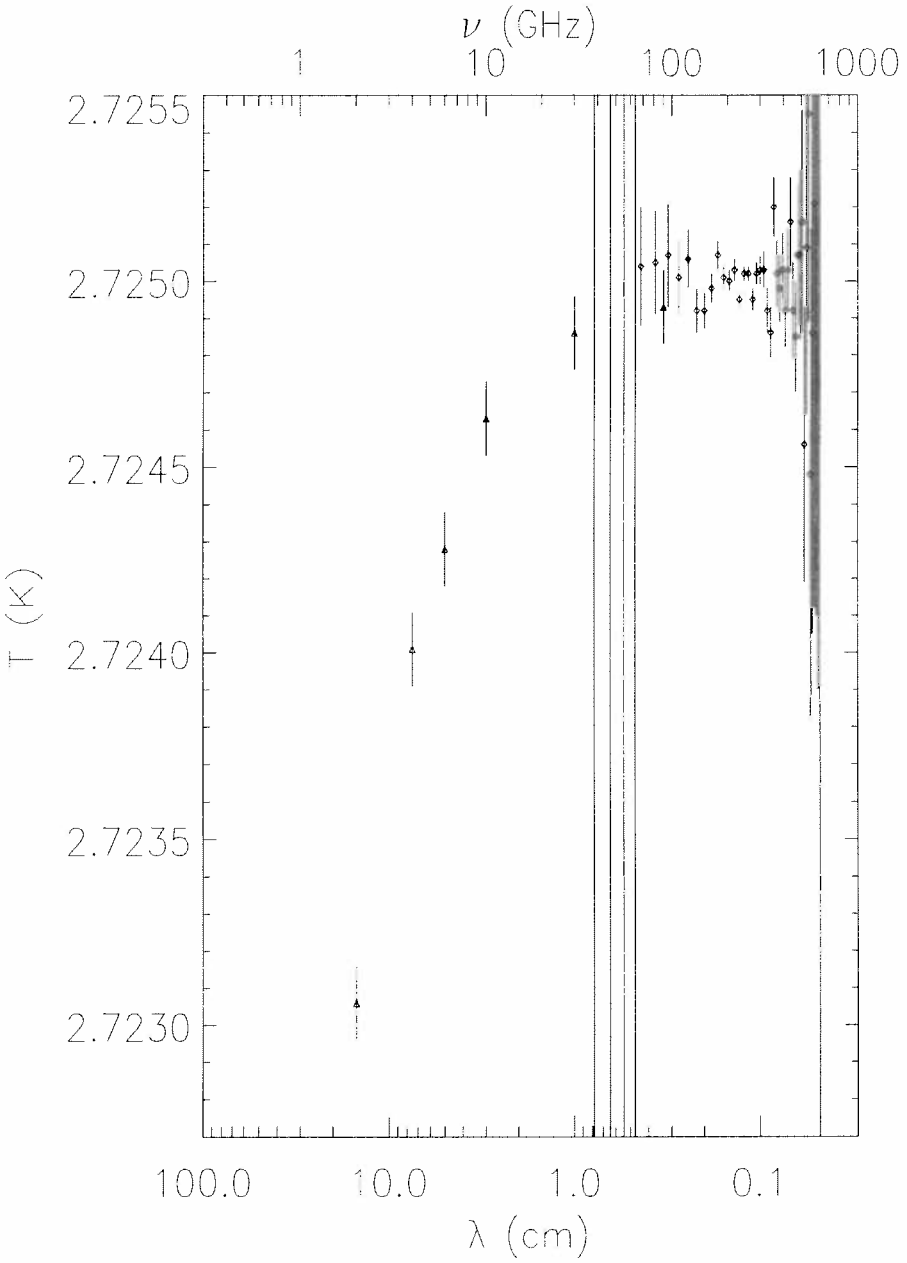

Figure 3: Values of the fractional energy injected in the radiation field at different epochs as obtained from the fit to the FIRAS data calibrated at 2.725 K jointed to future realistic ground and balloon data simulating the observation of a blackbody at 2.725 K. The solid line is the best-fit, the dashed lines are the upper and the lower limits at 95% CL.

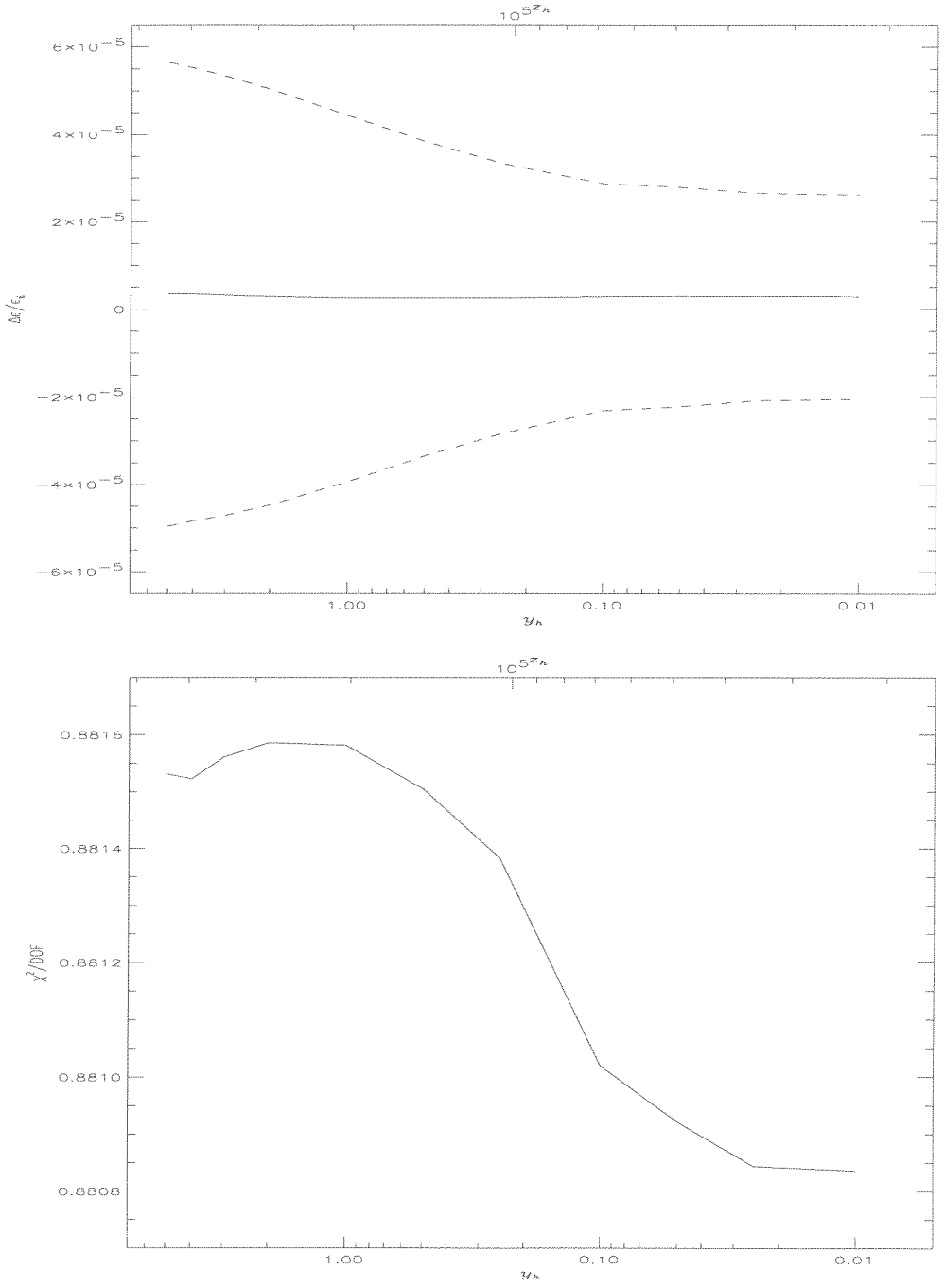

Figure 4: Values of χ^2/DOF for the fit to the FIRAS data calibrated at 2.725 K jointed to future realistic ground and balloon data simulating the observation of a blackbody at 2.725 K. We fit 59 data with 2 parameters: T_0 and $\Delta\epsilon/\epsilon_i$.

Figure 5: Values of the fractional energy injected in the radiation field at different epochs as obtained from the fit to the FIRAS data calibrated at 2.725 K jointed to possible ground and balloon data simulating the observation of a blackbody at 2.725 K with sensitivities 10 times better than those realistically expected. The solid line is the best-fit, the dashed lines are the upper and the lower limits at 95% CL.

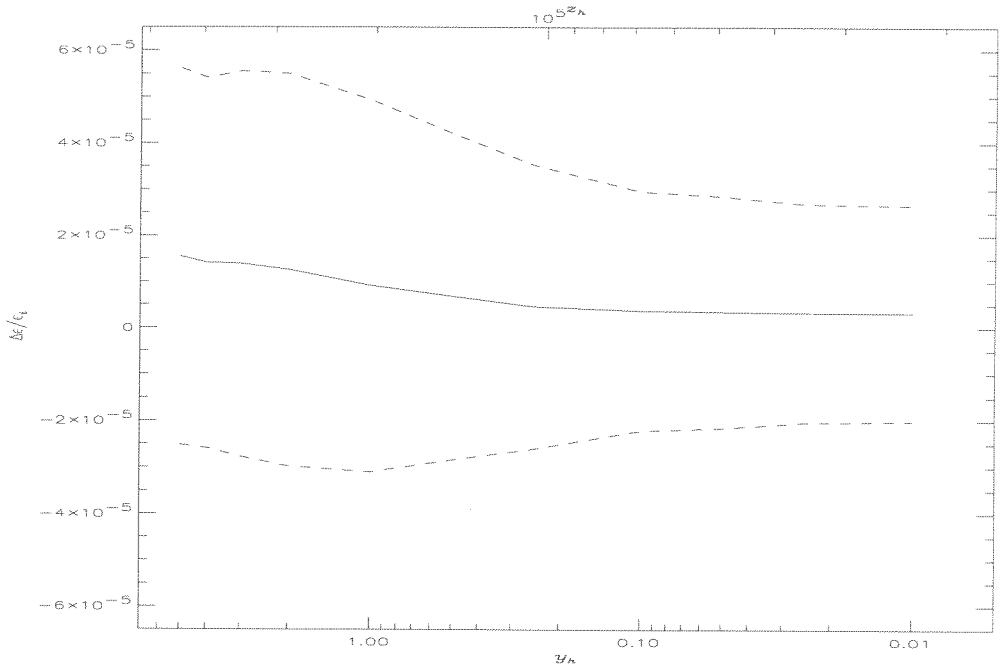

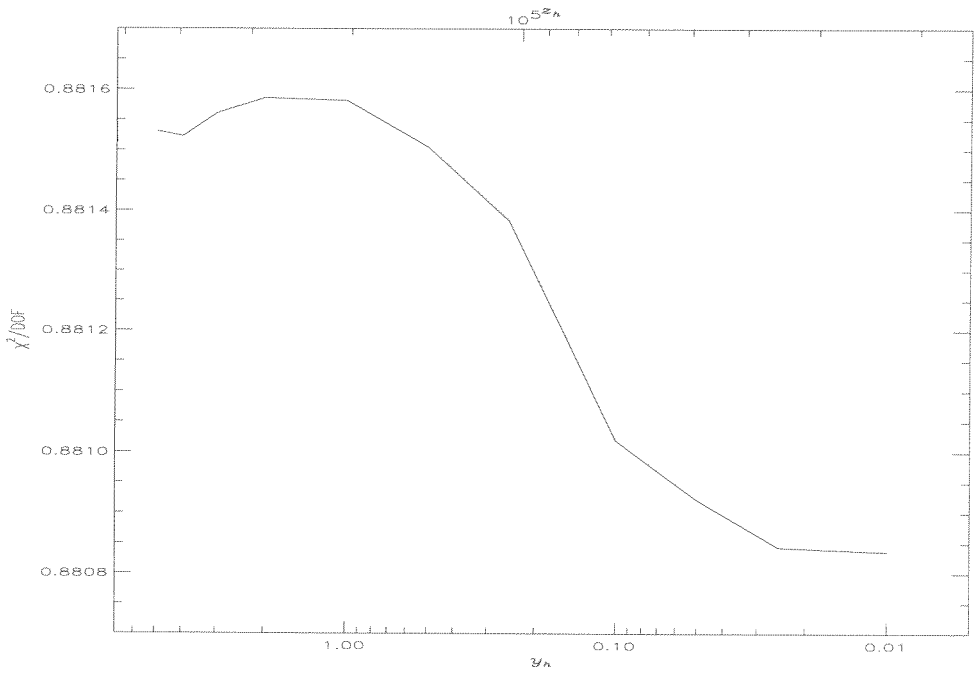

Figure 6: Values of χ^2/DOF for the fit to the FIRAS data calibrated at 2.725 K jointed to possible ground and balloon data simulating the observation of a blackbody at 2.725 K with sensitivities 10 times better than those realistically expected. We fit 59 data with 2 parameters: T_0 and $\Delta\epsilon/\epsilon_i$.

Figure 7: Values of the fractional energy injected in the radiation field at different epochs as obtained from the fit to the FIRAS data calibrated at 2.725 K jointed to simulated observations of a blackbody at 2.725 K with a sensitivity of a DIMES-like experiment. The solid line is the best-fit, the dashed lines are the upper and the lower limits at 95% CL.

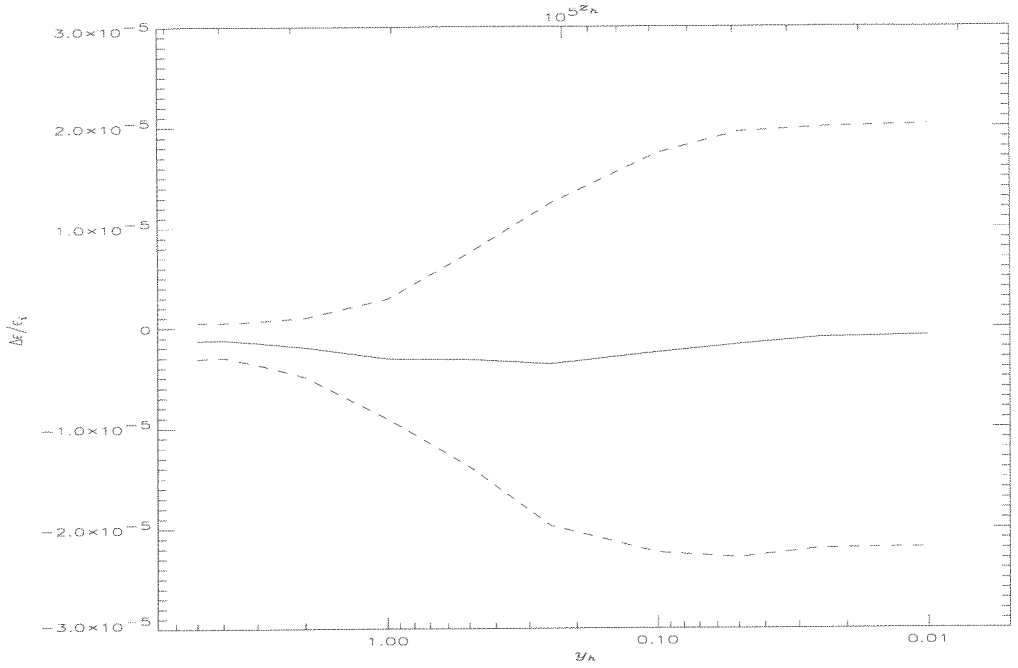

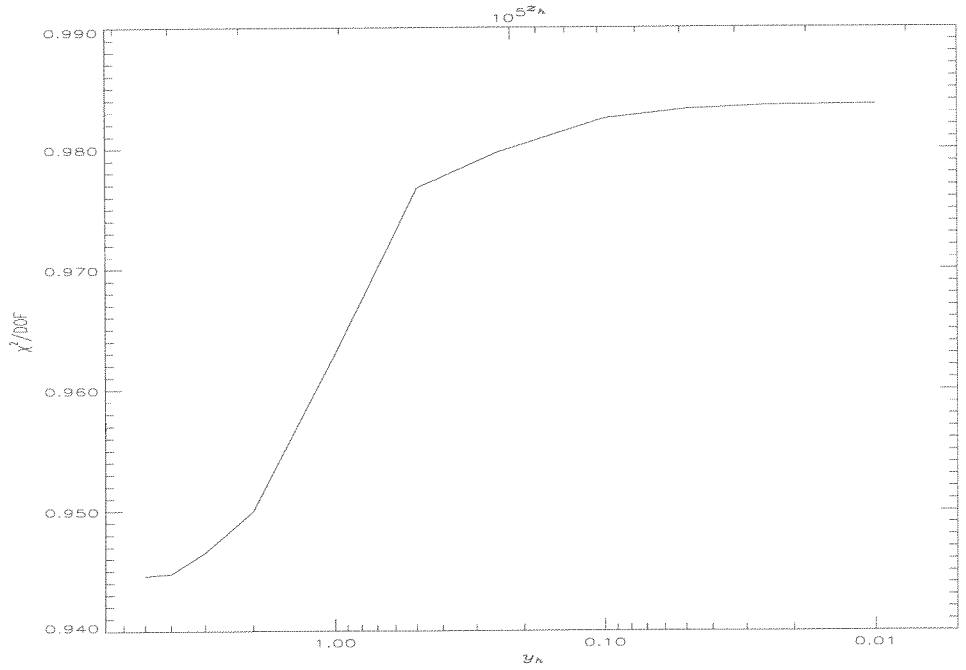

Figure 8: Values of χ^2/DOF for the fit to the FIRAS data calibrated at 2.725 K jointed to simulated observations of a blackbody at 2.725 K with a sensitivity of a DIMES-like experiment. We fit 53 data with 2 parameters: T_0 and $\Delta\epsilon/\epsilon_i$.

Figure 9: Values of the fractional energy injected in the radiation field at different epochs as obtained from the fit to the FIRAS data calibrated at 2.725 K jointed to simulated observations of a spectrum distorted at different cosmic epochs with $\Delta\epsilon/\epsilon_i = 2 \times 10^{-5}$ with a sensitivity of a DIMES-like experiment. The solid line is the best-fit, the dashed lines are the upper and the lower limits at 95% CL. The fit is performed assuming to know the heating epoch.

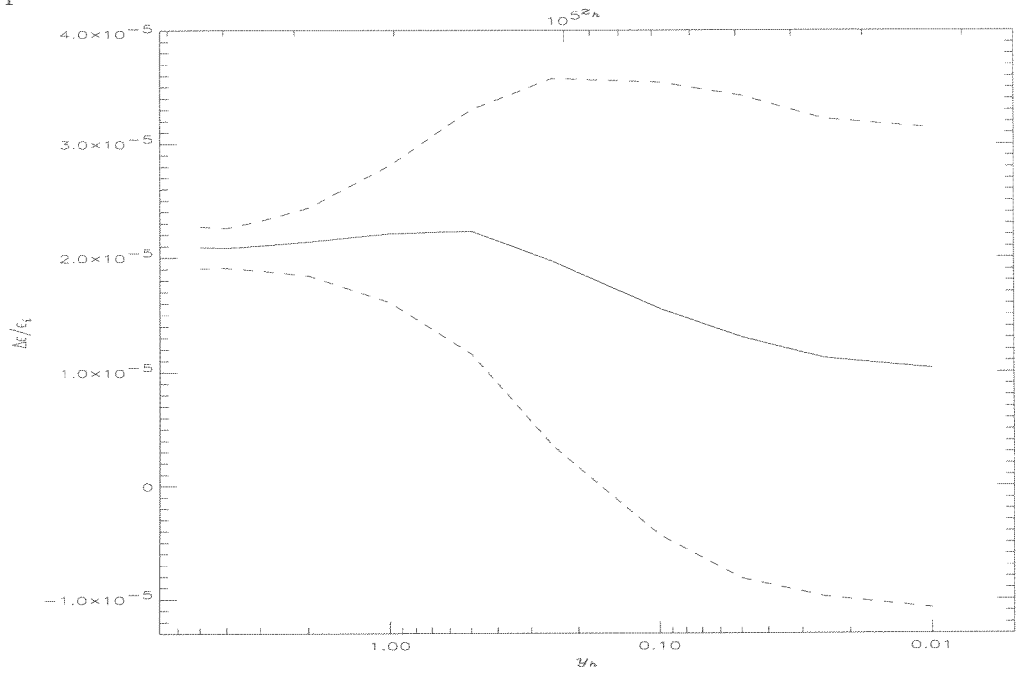

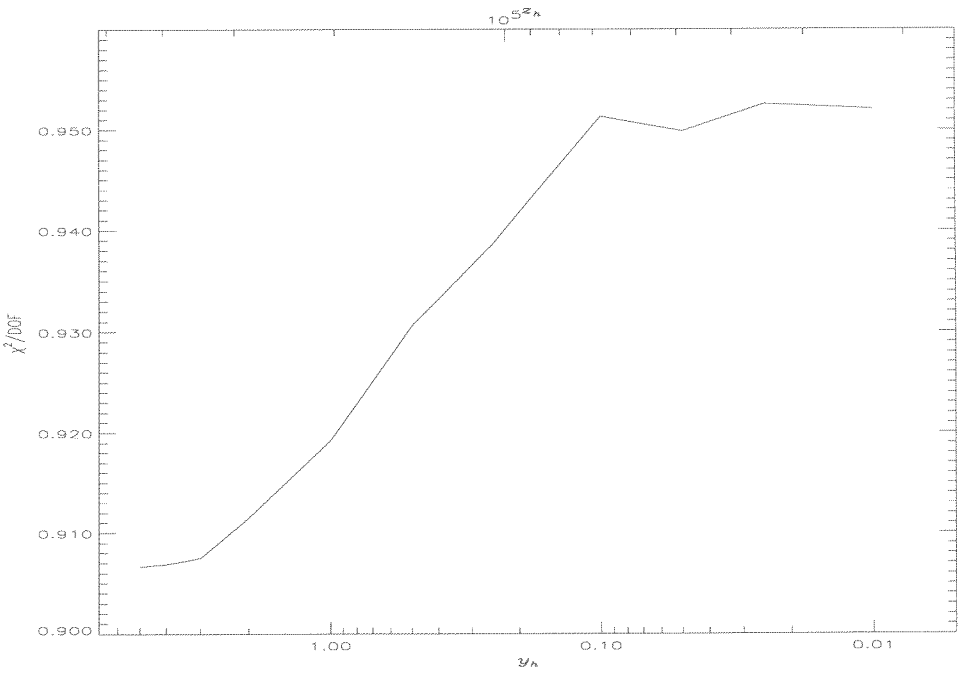

Figure 10: Values of χ^2/DOF for the fit to the FIRAS data calibrated at 2.725 K jointed to simulated observations of a spectrum distorted at different cosmic epochs with $\Delta\epsilon/\epsilon_i = 2 \times 10^{-5}$ with a sensitivity of a DIMES-like experiment. We fit 53 data with 2 parameters, T_0 and $\Delta\epsilon/\epsilon_i$, assuming to know the heating epoch.

Figure 11: Values of the fractional energy injected in the radiation field at different epochs as obtained from the fit to the FIRAS data calibrated at 2.725 K jointed to simulated observations of a spectrum distorted at $y_h = 5$ with $\Delta\epsilon/\epsilon_i = 2 \times 10^{-5}$ with a sensitivity of a DIMES-like experiment. The solid line is the best-fit, the dashed lines are the upper and the lower limits at 95% CL. The fit is performed without assumptions on the heating epoch.

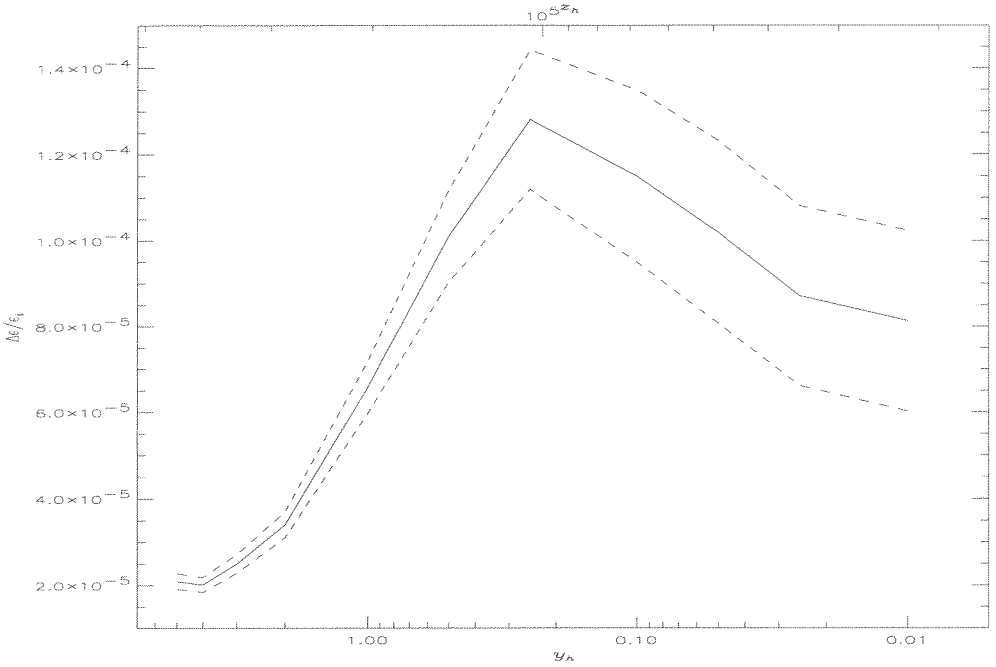

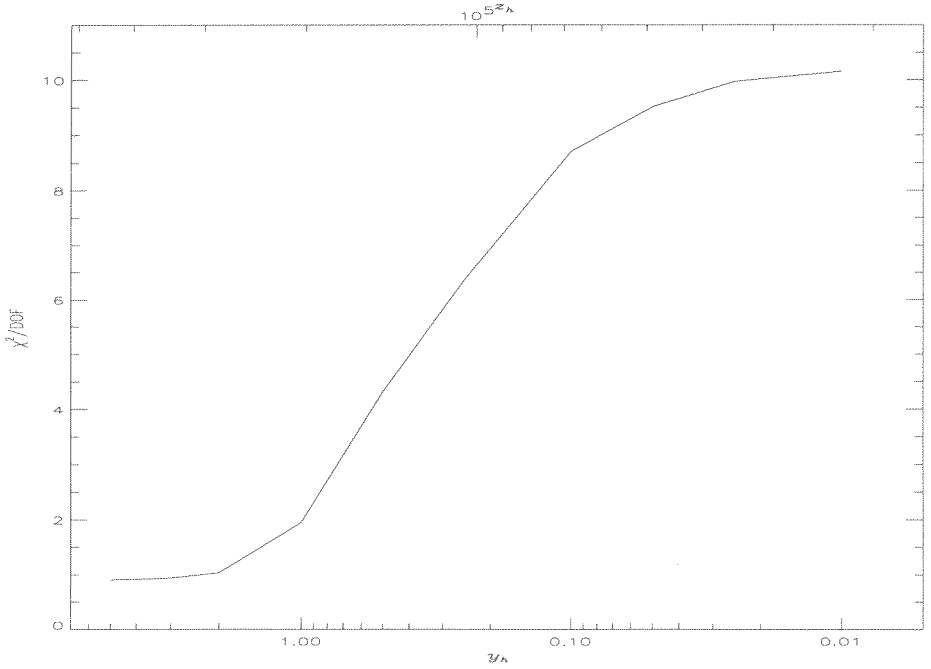

Figure 12: Values of χ^2/DOF for the fit to the FIRAS data calibrated at 2.725 K jointed to simulated observations of a spectrum distorted at $y_h = 5$ with $\Delta\epsilon/\epsilon_i = 2 \times 10^{-5}$ with a sensitivity of a DIMES-like experiment. We fit 53 data with 2 parameters, T_0 and $\Delta\epsilon/\epsilon_i$, without assumptions on the heating epoch.

Figure 13: Recovered value of the injected energy at a given epoch y_h (solid line) and limits at 95% CL (dashed lines) by allowing also for a second heating occurring at $y_h \ll 1$. The input spectrum is based on FIRAS data calibrated at 2.725 K and, at longer wavelengths, by a spectrum distorted by two processes, the first at $y_h = 5$ and the second at $y_h \ll 1$ the both with $\Delta\epsilon/\epsilon_i = 5 \times 10^{-6}$, as observed by a DIMES-like experiment.

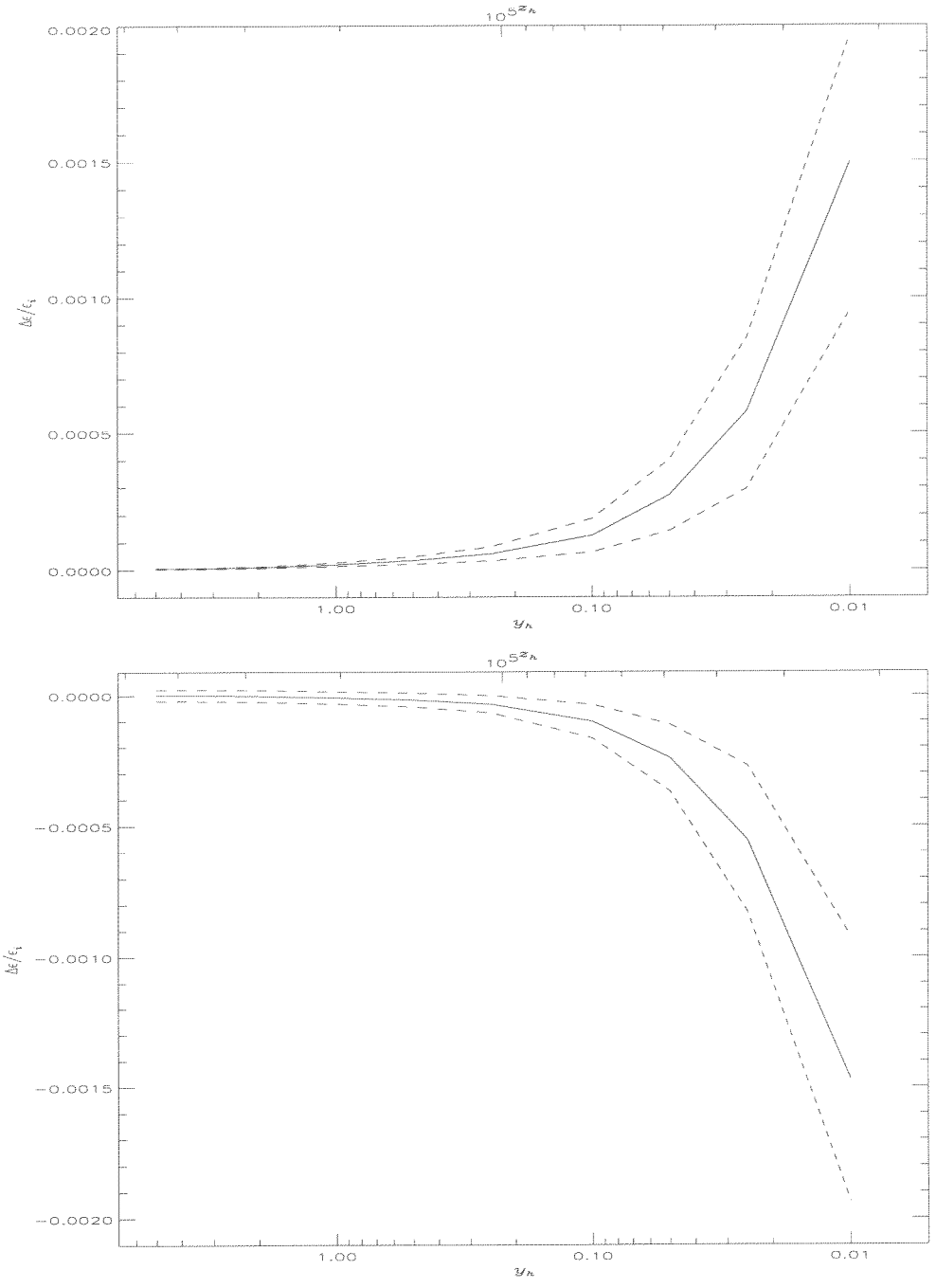

Figure 14: Recovered value of the injected energy at $y_h \ll 1$ (solid line) and limits at 95% CL (dashed lines) by allowing also for a second heating occurring at a given epoch y_h. The input spectrum is based on FIRAS data calibrated at 2.725 K and, at longer wavelengths, by a spectrum distorted by two processes, the first at $y_h = 5$ and the second at $y_h \ll 1$ the both with $\Delta\epsilon/\epsilon_i = 5 \times 10^{-6}$, as observed by a DIMES-like experiment.

Figure 15: Values of χ^2/DOF for the best fit to the FIRAS data calibrated at 2.725 K jointed, at longer wavelengths, by a spectrum distorted by two processes, the first at $y_h = 5$ and the second at $y_h \ll 1$ the both with $\Delta\epsilon/\epsilon_i = 5 \times 10^{-6}$, as observed by a DIMES-like experiment. We fit 53 data with 3 parameters, T_0 and the two values of $\Delta\epsilon/\epsilon_i$, the latter referring to a possible earlier process occurring at the given value of y_h, the former referring to a process at $y_h \ll 1$.

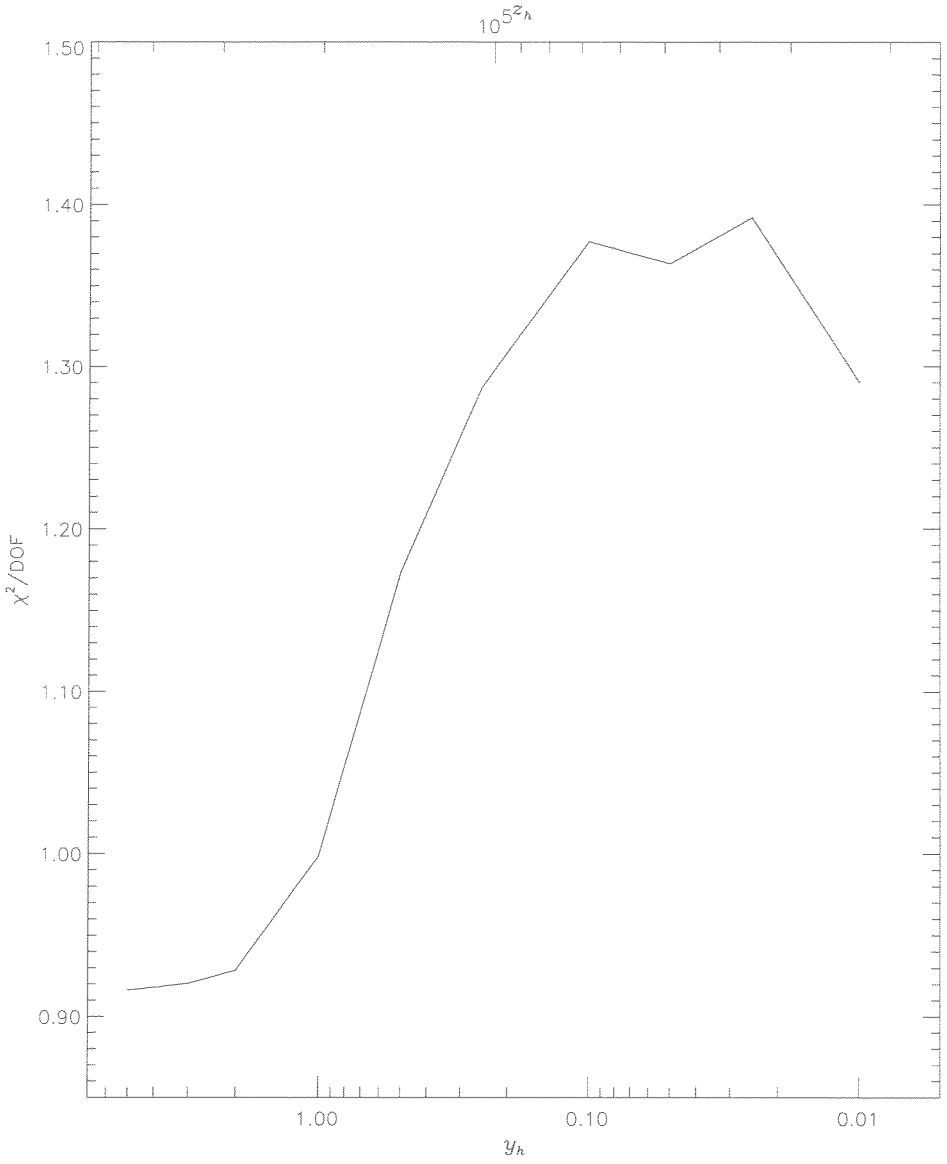

Figure 16: Upper (top panel) and lower (bottom panel) limits at 95% CL on the amount of the energy injected at $z_h \leq z_1$ with the extension to $z_1 \leq z_h < 0.9 z_{therm}$ as obtained with the FIRAS data alone (dashed lines) and by adding simulated data from a DIMES-like experiment in the case of the observation of a not distorted spectrum at 2.725 K (solid lines). We assume a single energy injection process at known epoch.

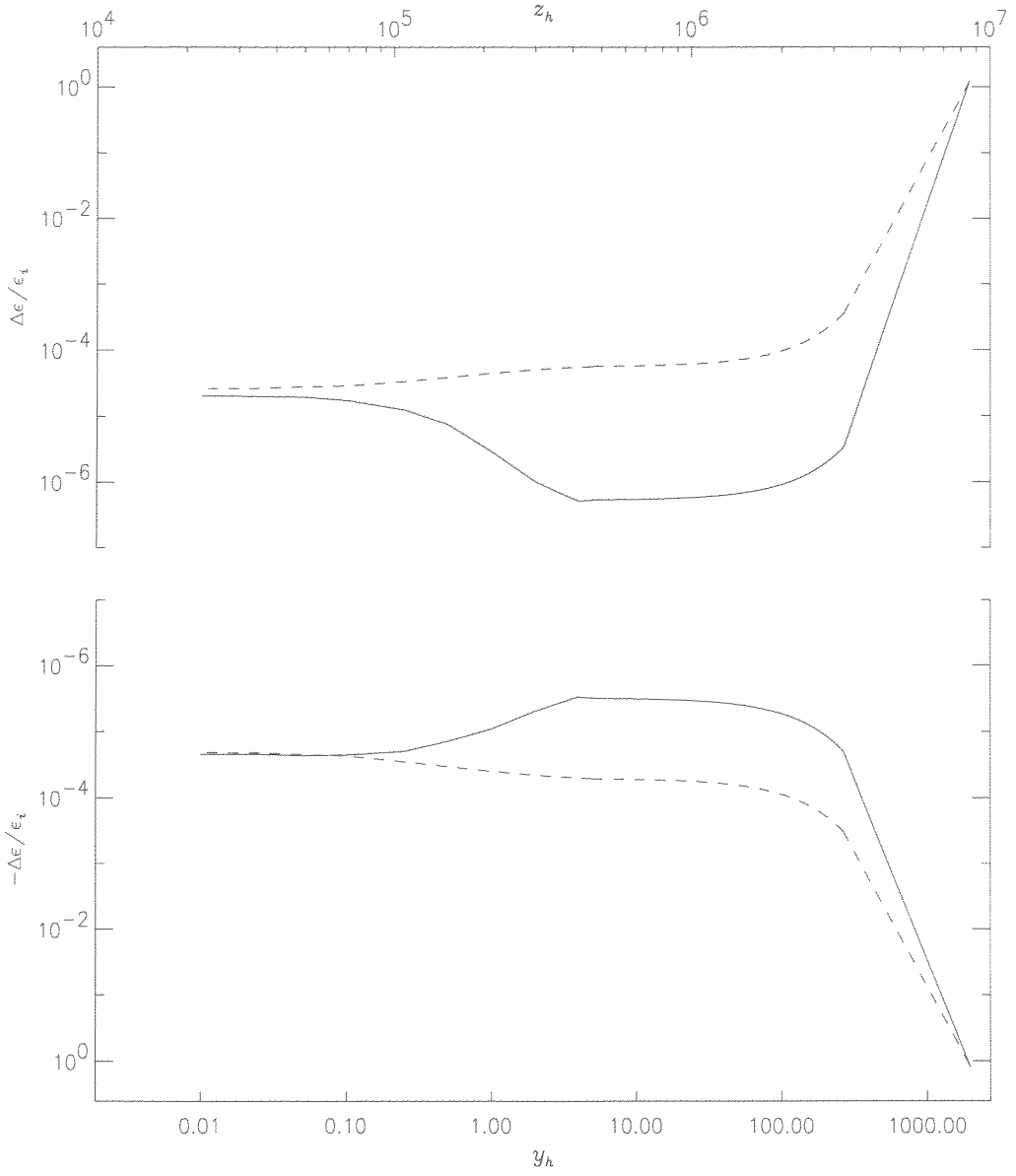

Figure 17: Best fit (dotted line) and upper and lower limits at 95% CL (solid lines) on the amount of the energy injected at $z_h \leq z_1$ with the extension to $z_1 \leq z_h < 0.9 z_{therm}$ as obtained from the FIRAS data jointed to longer wavelength simulated data from a DIMES-like experiment in the case of the observation of a spectrum distorted with $\Delta\epsilon/\epsilon_i = 2 \times 10^{-5}$ The arrows indicate that the lower limits on $\Delta\epsilon/\epsilon_i$ become negative at low y_h and cannot be plotted in logarithmic scale (see Fig.s 9 and 10). We assume a single energy injection process at known epoch.

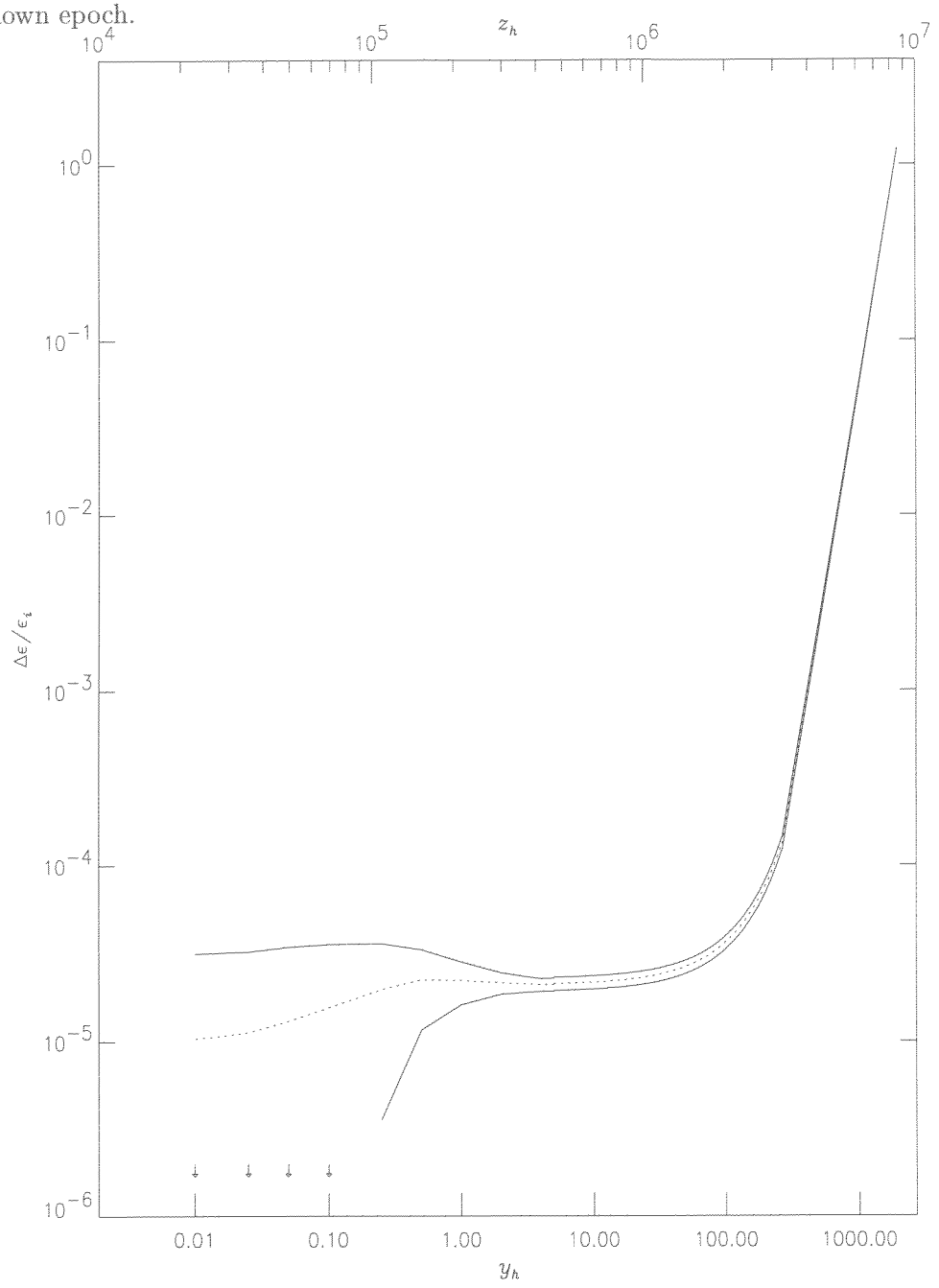

Figure 18: The same as in Fig. 17, but for $\Delta\epsilon/\epsilon_i = 5 \times 10^{-6}$.

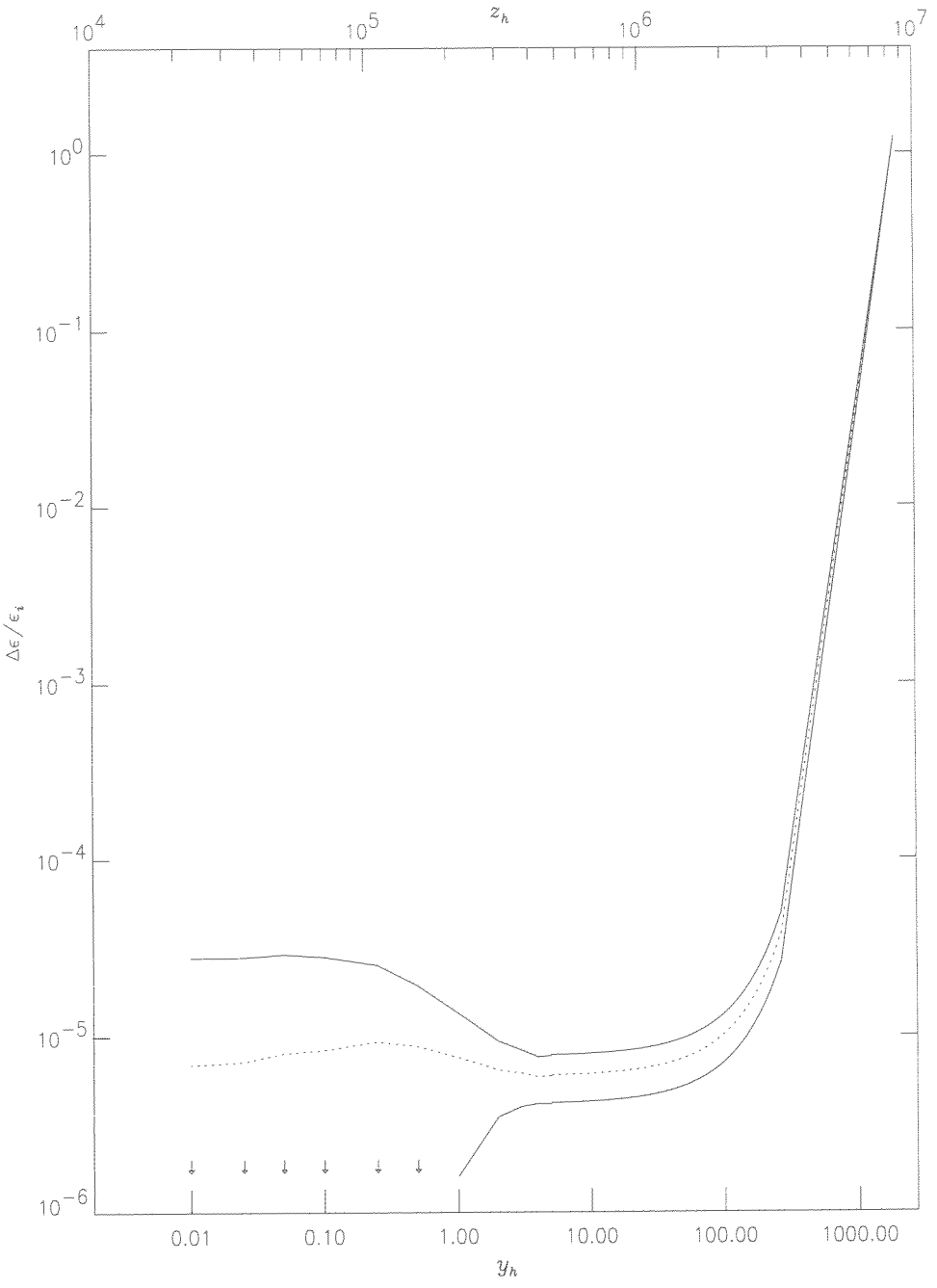

Figure 19: Wavelength of the minimum of the CMB absolute temperature for a Bose-Einstein distortion as a function of $\widehat{\Omega}_b$.

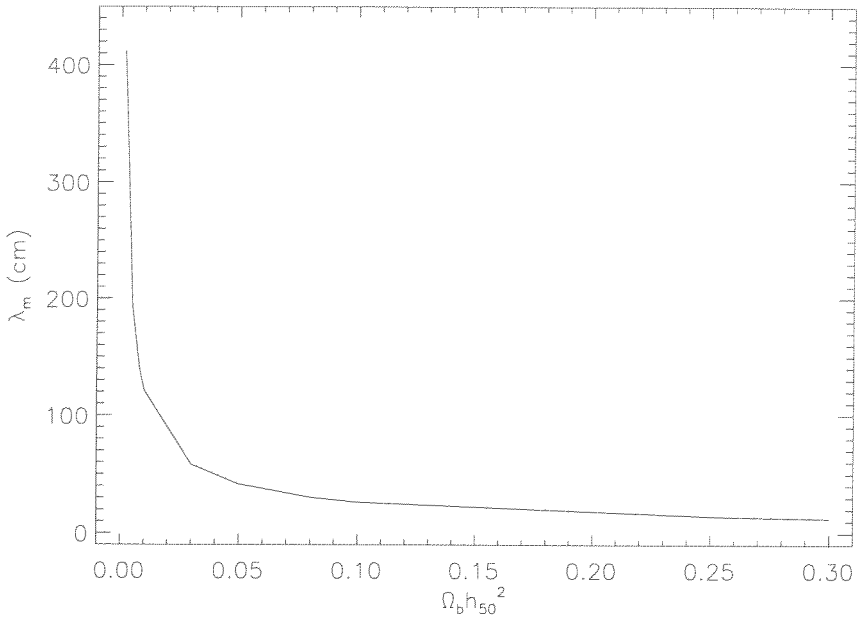

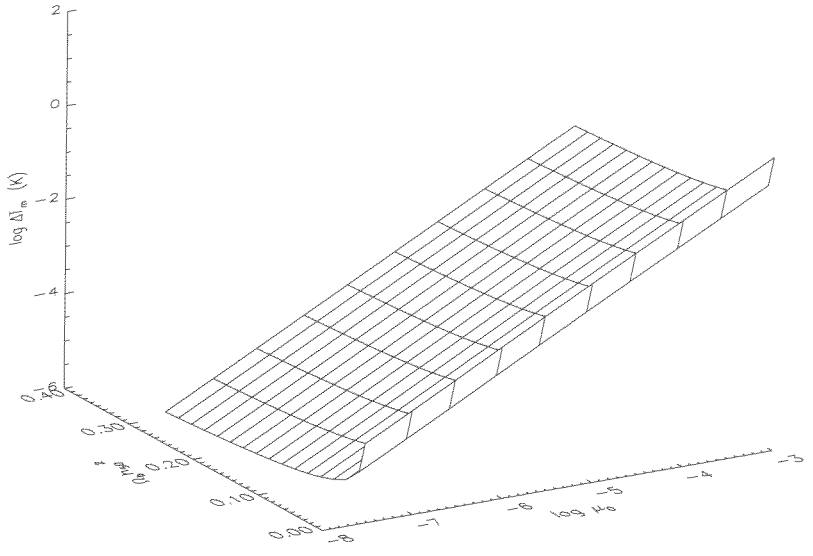

Figure 20: Amplitude of the maximum decrement of the CMB absolute temperature for a Bose-Einstein distortion as a function of μ_0 and of $\widehat{\Omega}_b$.

Figure 21: Amplitude of the maximum decrement of the CMB absolute temperature for a Bose-Einstein distortion as a function of $\widehat{\Omega}_b$ for some values of μ_0.

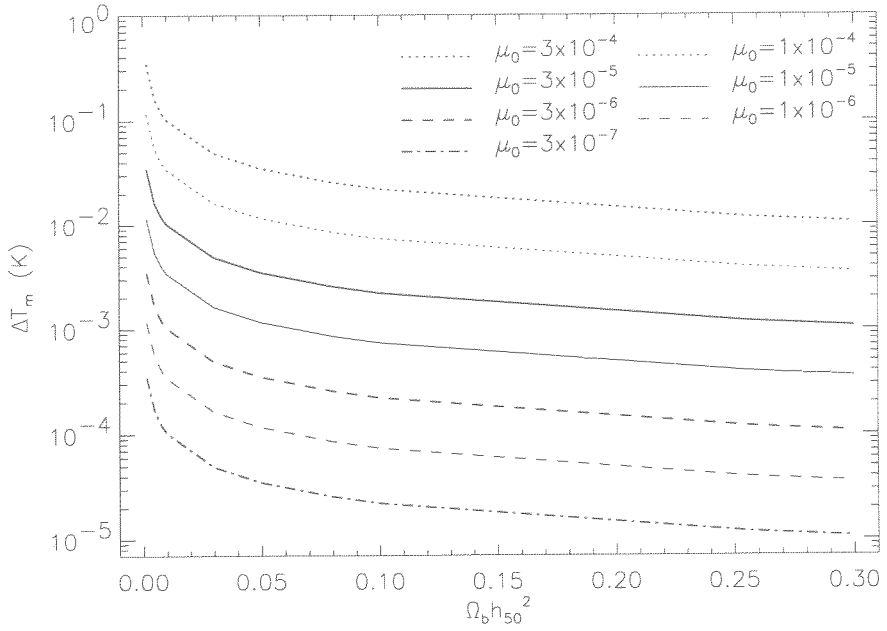

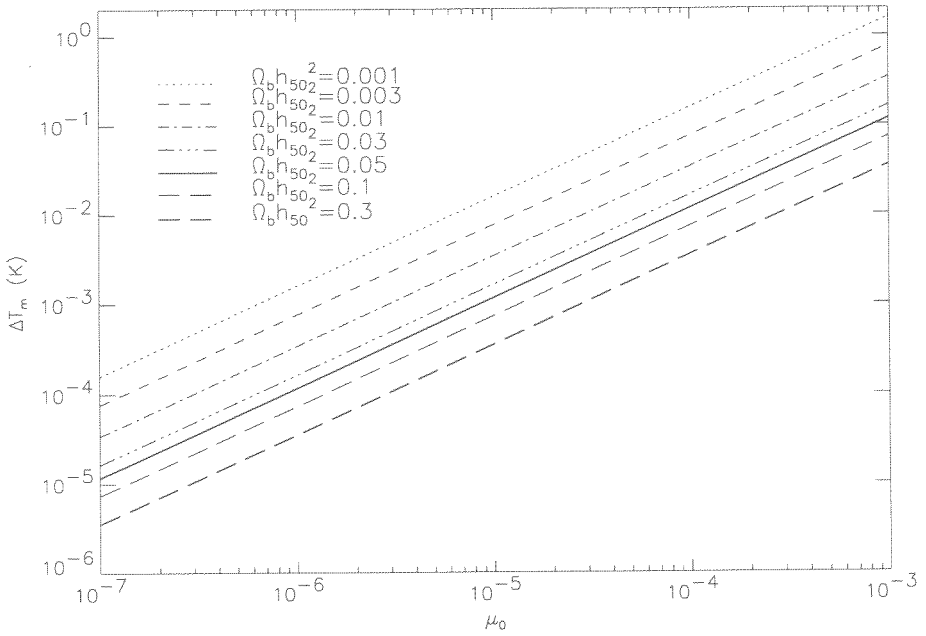

Figure 22: Amplitude of the maximum decrement of the CMB absolute temperature for a Bose-Einstein distortion as a function of μ_0 for some values of $\widehat{\Omega}_b$.

A Auxiliary figures of the fits of the simulated data

We report here the figures for the whole set of the fits to the available measures of the CMB absolute temperature.

The best fit values and the 95% CL limits on $\Delta\epsilon/\epsilon_i$ as well as the χ^2/DOF value corresponding to the best fit values are reported as functions of y_h. We report also in the plots the values of z_h corresponding to y_h as obtained by a simple power law approximation of eq. (2). See Tab. 8 for a more precise correspondence.

The results reported in the figures refer to the case $\Omega_b = 0.05$.

	$\hat{\Omega}_b$		
y_h	0.01	0.05	0.1
5.000	9.65×10^5	4.33×10^5	3.07×10^5
4.000	8.63×10^5	3.88×10^5	2.75×10^5
3.000	7.48×10^5	3.36×10^5	2.38×10^5
2.000	6.11×10^5	2.75×10^5	1.95×10^5
1.000	4.33×10^5	1.95×10^5	1.3×910^5
0.500	3.07×10^5	1.39×10^5	0.99×10^5
0.250	2.18×10^5	0.99×10^5	0.71×10^5
0.100	1.39×10^5	0.63×10^5	0.45×10^5
0.050	0.99×10^5	0.45×10^5	0.33×10^5
0.025	0.71×10^5	0.33×10^5	0.24×10^5
0.010	0.45×10^5	0.21×10^5	0.15×10^5

Table 1: Redshift corresponding to y_h for $\Omega = 1$, $H_0 = 50$ km/s/Mpc, $T_e/T_r = 1$, $T_0 = 2.725$ K and three massless neutrino species ($\kappa \simeq 1.68$),

Figure 23: Values of the fractional energy injected in the radiation field at different epochs as obtained from the fit to the FIRAS data calibrated at 2.725 K jointed to simulated observations of a spectrum distorted at $y_h = 1.5$ with $\Delta\epsilon/\epsilon_i = 2 \times 10^{-5}$ with a sensitivity of a DIMES-like experiment. The solid line is the best-fit, the dashed lines are the upper and the lower limits at 95% CL. The fit is performed without assumptions on the heating epoch.

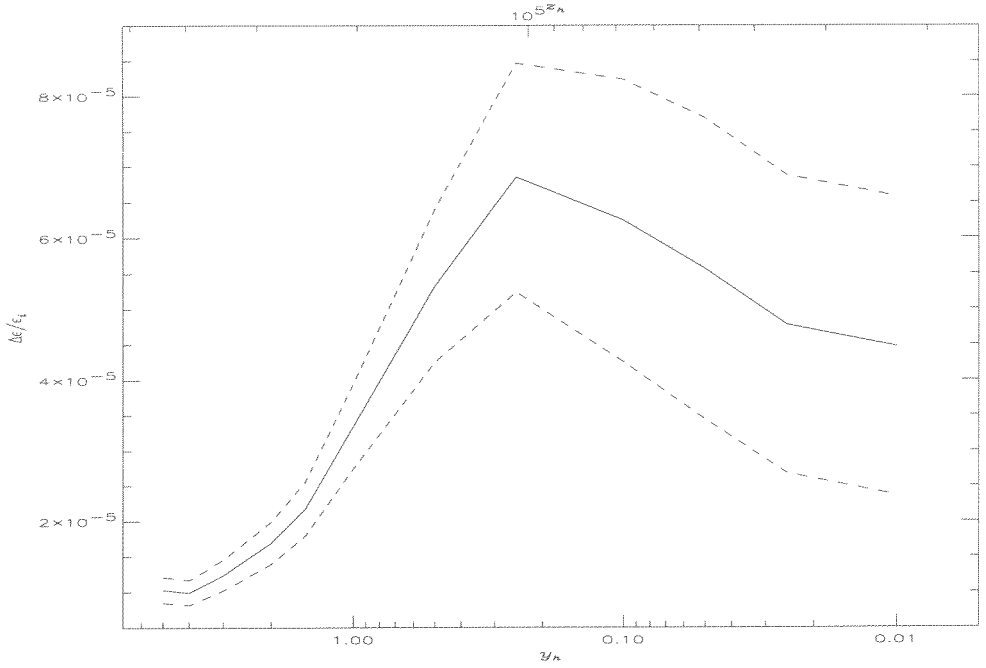

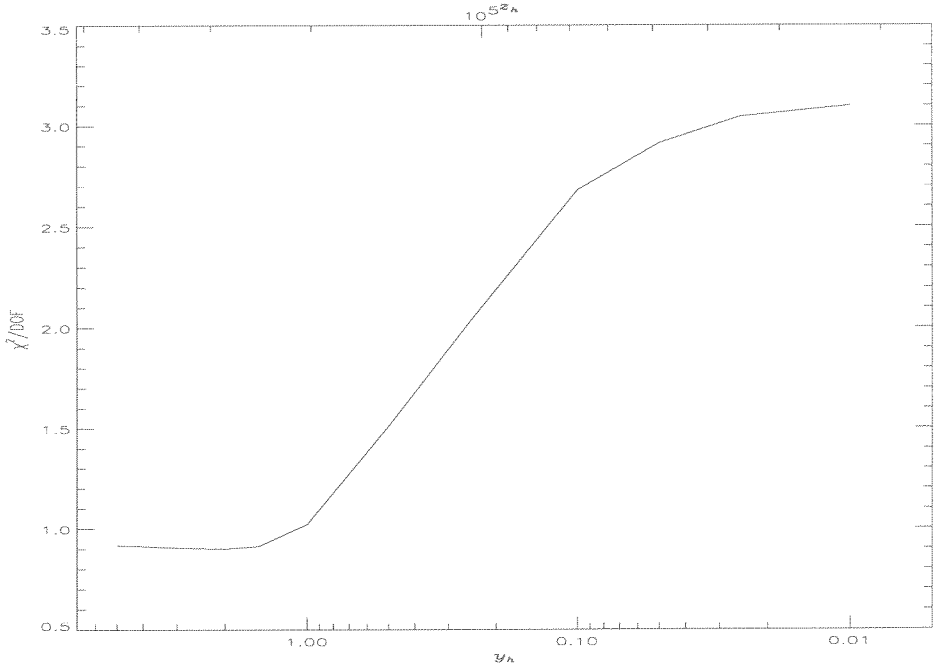

Figure 24: Values of χ^2/DOF for the fit to the FIRAS data calibrated at 2.725 K jointed to simulated observations of a spectrum distorted at $y_h = 1.5$ with $\Delta\epsilon/\epsilon_i = 2 \times 10^{-5}$ with a sensitivity of a DIMES-like experiment. We fit 53 data with 2 parameters, T_0 and $\Delta\epsilon/\epsilon_i$, without assumptions on the heating epoch.

Figure 25: The same as in Fig. 23 but for a spectrum distorted at $y_h = 0.01$.

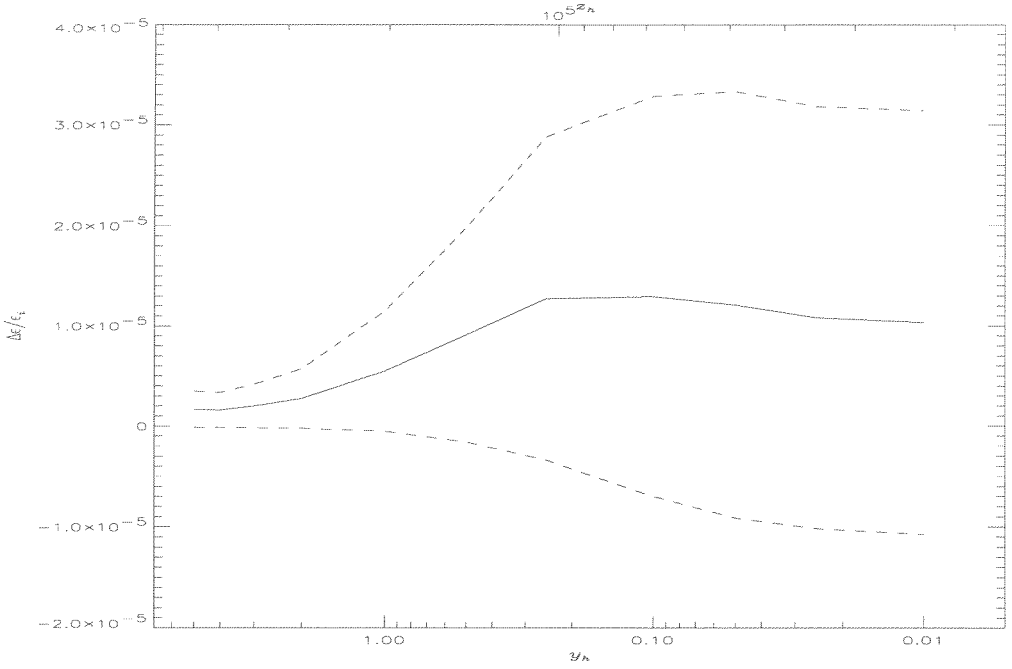

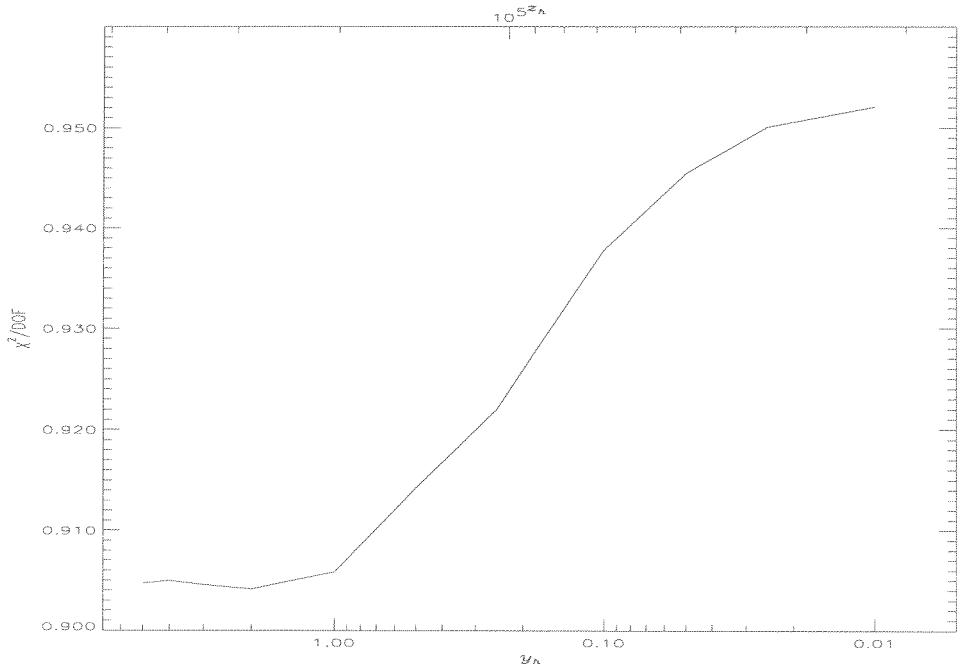

Figure 26: The same as in Fig. 24 but for a spectrum distorted at $y_h = 0.01$.

Figure 27: Values of the fractional energy injected in the radiation field at different epochs as obtained from the fit to the FIRAS data calibrated at 2.725 K jointed to simulated observations of a spectrum distorted at different cosmic epochs with $\Delta\epsilon/\epsilon_i = 5 \times 10^{-6}$ with a sensitivity of a DIMES-like experiment. The solid line is the best-fit, the dashed lines are the upper and the lower limits at 95% CL. The fit is performed assuming to know the heating epoch.

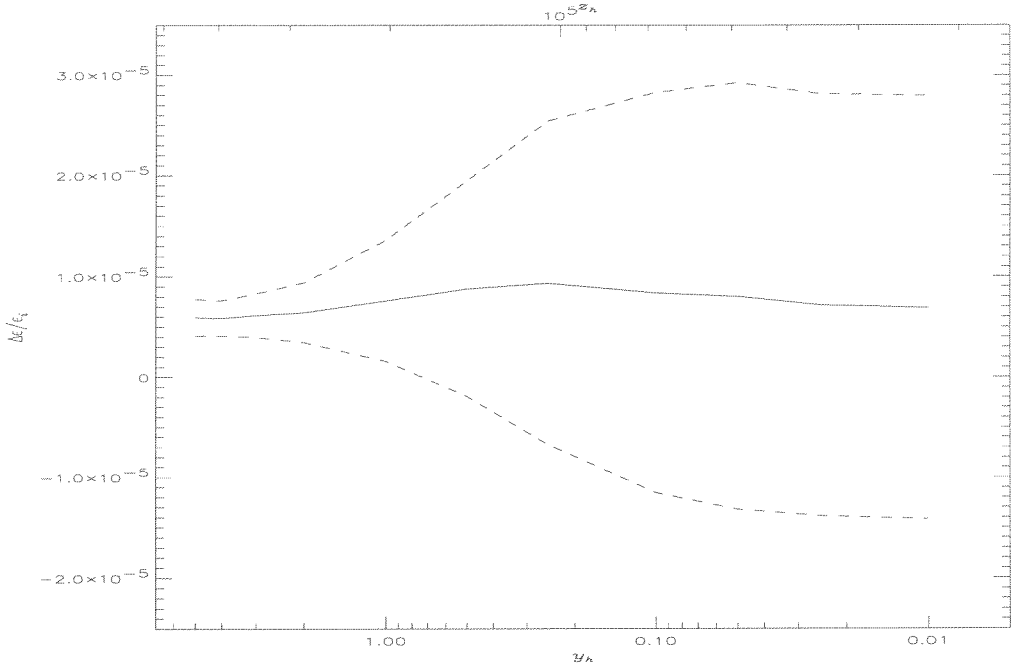

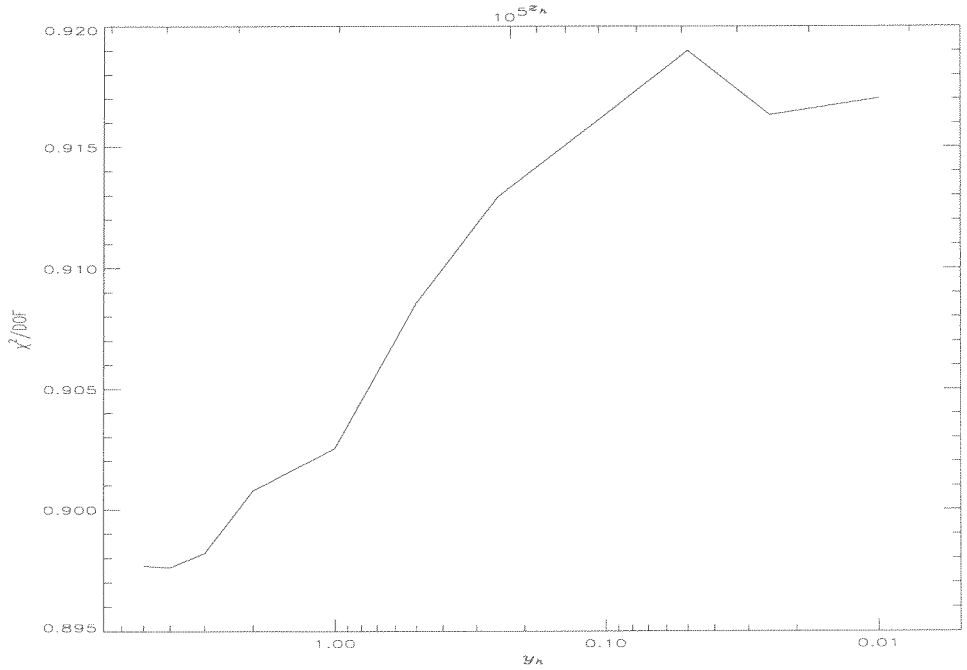

Figure 28: Values of χ^2/DOF for the fit to the FIRAS data calibrated at 2.725 K jointed to simulated observations of a spectrum distorted at different cosmic epochs with $\Delta\epsilon/\epsilon_i = 5 \times 10^{-6}$ with a sensitivity of a DIMES-like experiment. We fit 53 data with 2 parameters, T_0 and $\Delta\epsilon/\epsilon_i$, assuming to know the heating epoch.

Figure 29: Values of the fractional energy injected in the radiation field at different epochs as obtained from the fit to the FIRAS data calibrated at 2.725 K jointed to simulated observations of a spectrum distorted at $y_h = 5$ with $\Delta\epsilon/\epsilon_i = 5 \times 10^{-6}$ with a sensitivity of a DIMES-like experiment. The solid line is the best-fit, the dashed lines are the upper and the lower limits at 95% CL. The fit is performed without assumptions on the heating epoch.

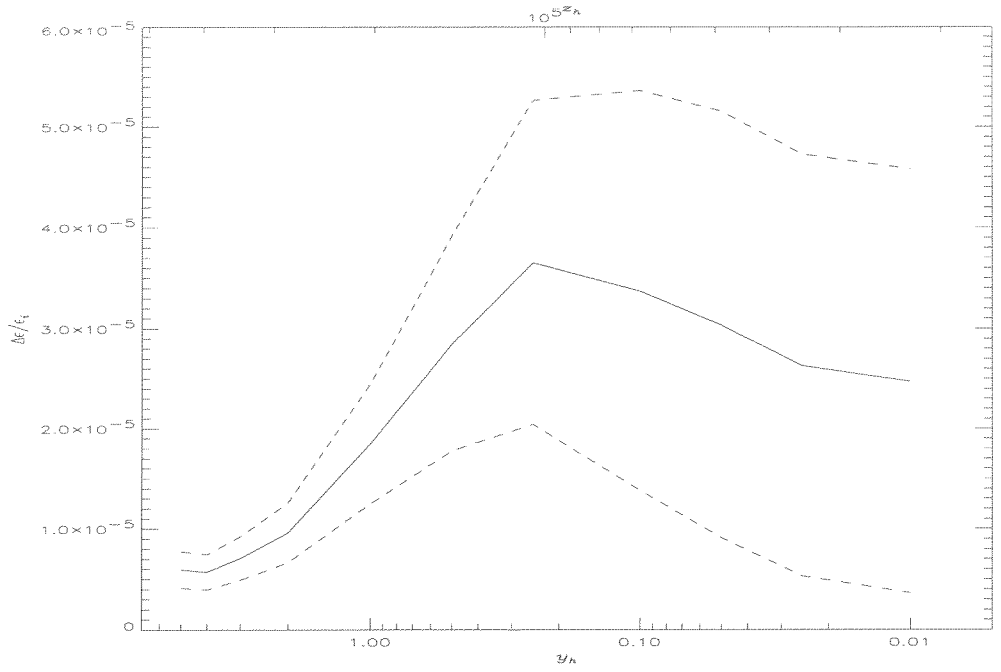

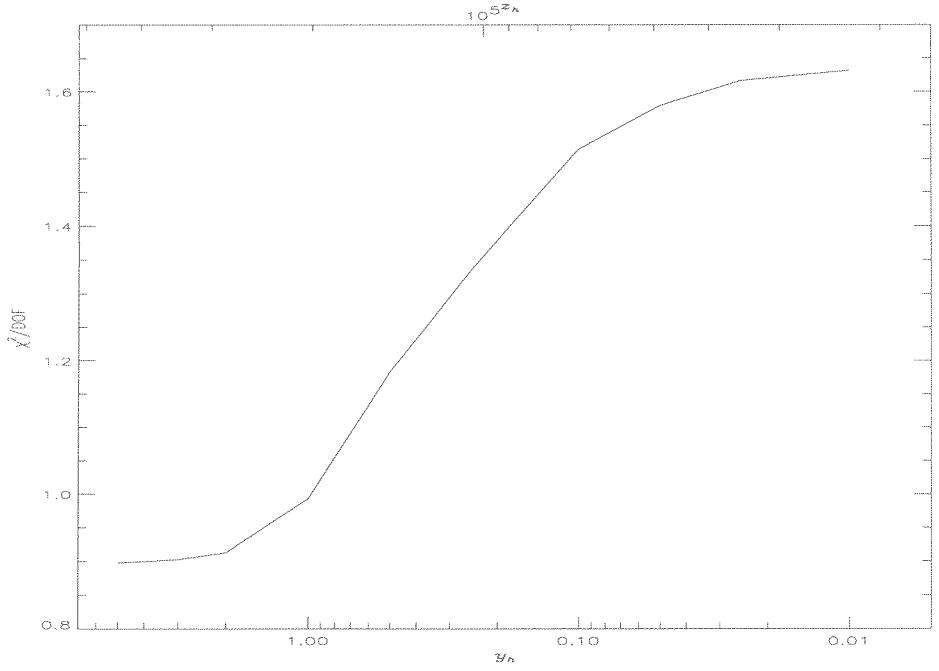

Figure 30: Values of χ^2/DOF for the fit to the FIRAS data calibrated at 2.725 K jointed to simulated observations of a spectrum distorted at $y_h = 5$ with $\Delta\epsilon/\epsilon_i = 5 \times 10^{-6}$ with a sensitivity of a DIMES-like experiment. We fit 53 data with 2 parameters, T_0 and $\Delta\epsilon/\epsilon_i$, without assumptions on the heating epoch.

Figure 31: The same as in Fig. 29 but for a spectrum distorted at $y_h = 1.5$.

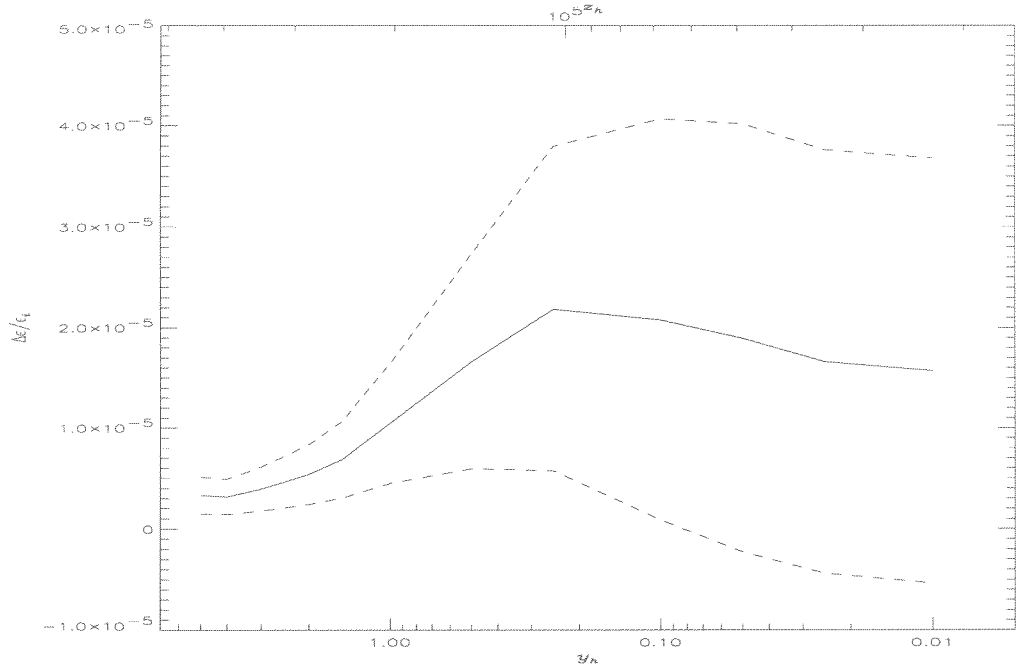

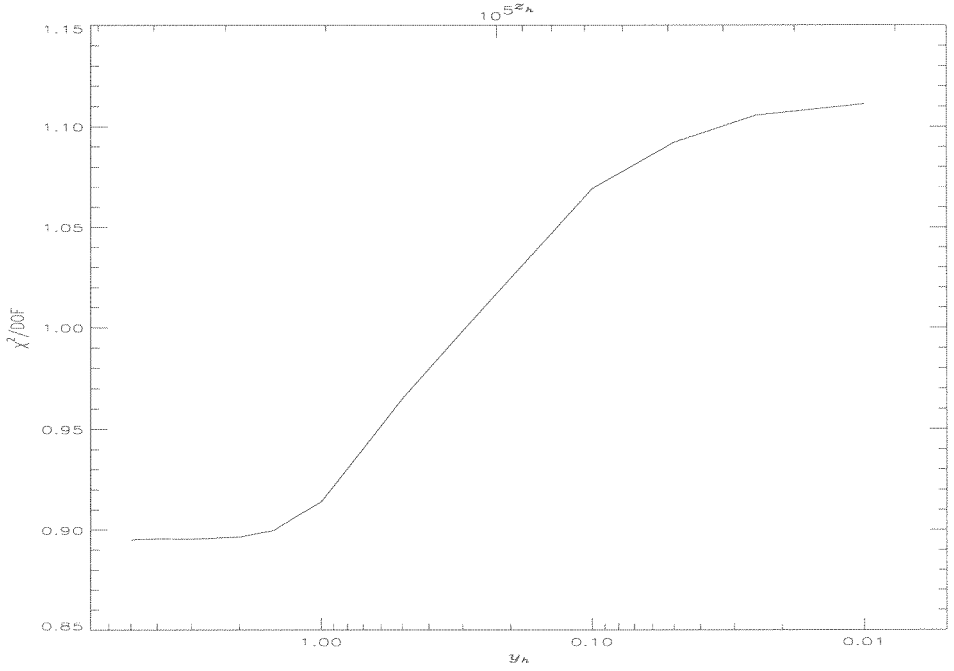

Figure 32: The same as in Fig. 30 but for a spectrum distorted at $y_h = 1.5$.

Figure 33: The same as in Fig. 29 but for a spectrum distorted at $y_h = 0.01$.

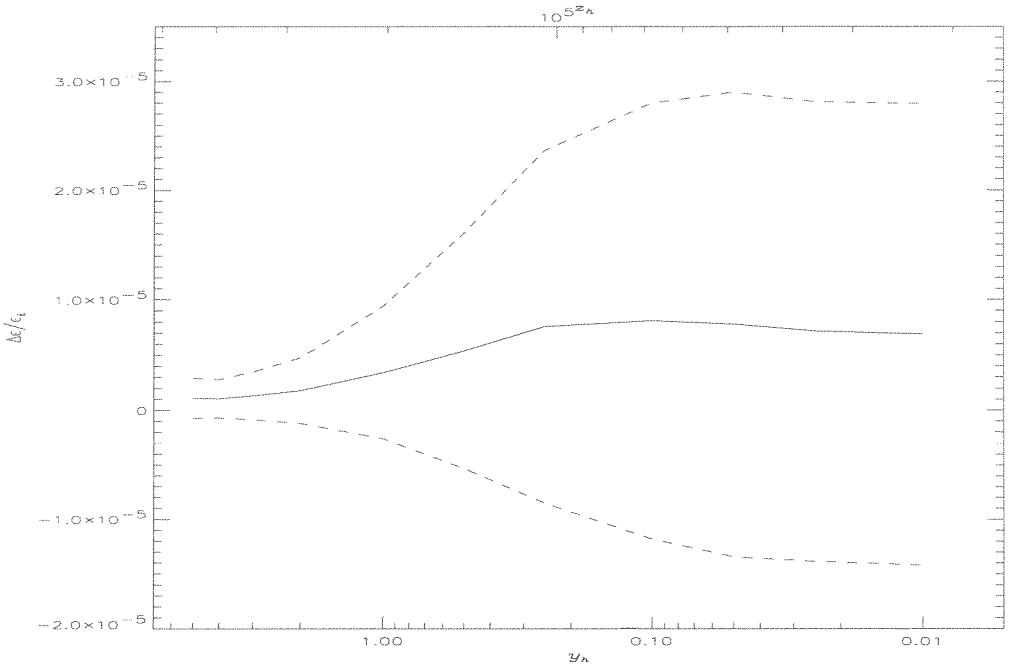

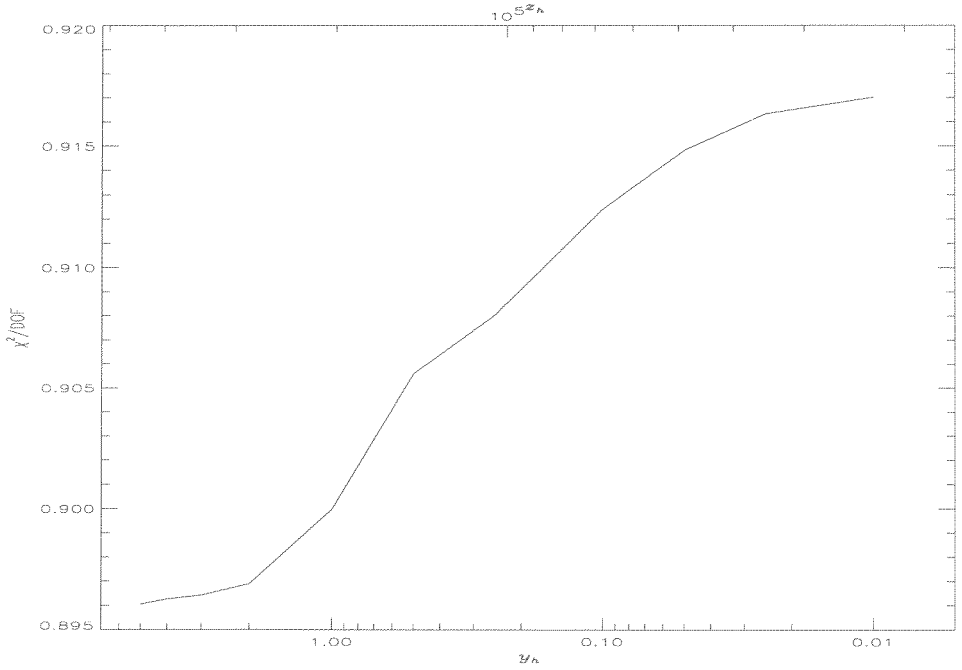

Figure 34: The same as in Fig. 30 but for a spectrum distorted at $y_h = 0.01$.

Figure 35: Values of the fractional energy injected in the radiation field at different epochs as obtained from the fit to the FIRAS data calibrated at 2.725 K jointed to simulated observations of a spectrum distorted at different cosmic epochs with $\Delta\epsilon/\epsilon_i = 2 \times 10^{-6}$ with a sensitivity of a DIMES-like experiment. The solid line is the best-fit, the dashed lines are the upper and the lower limits at 95% CL. The fit is performed assuming to know the heating epoch.

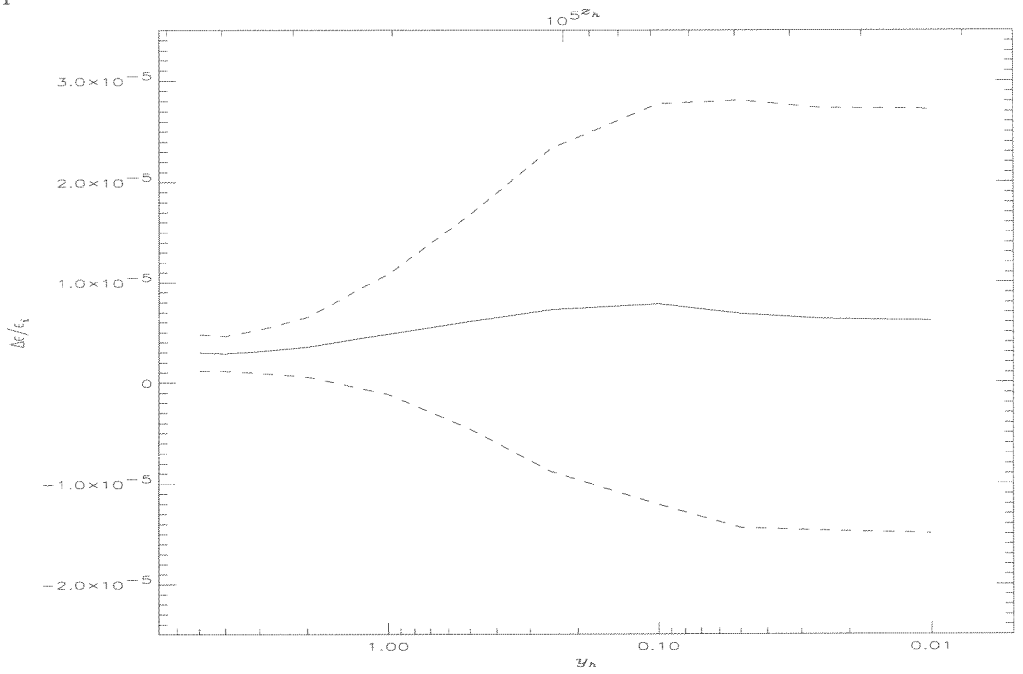

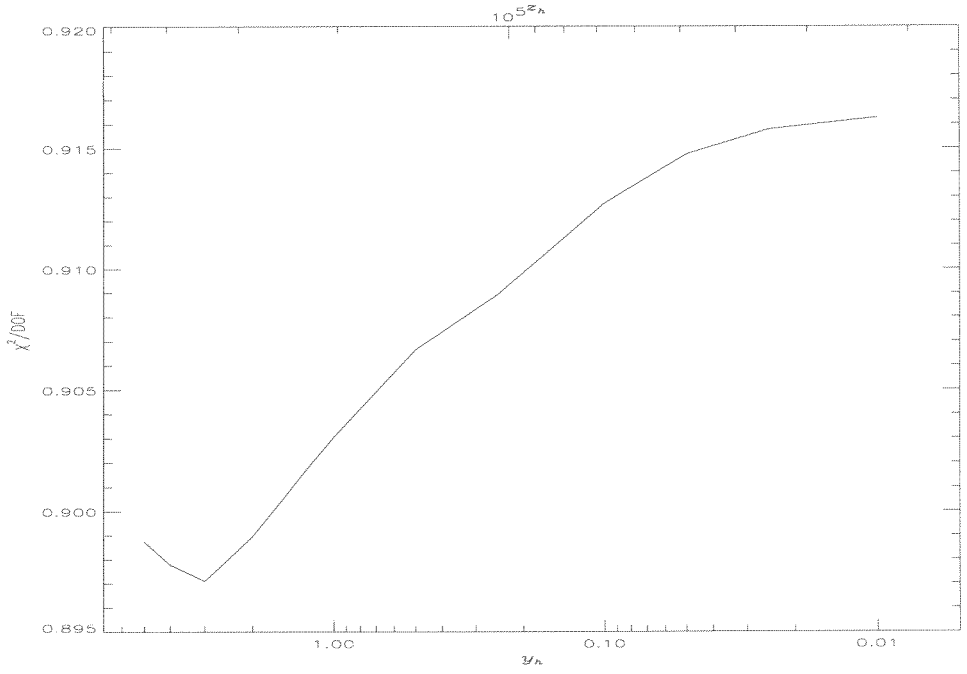

Figure 36: Values of χ^2/DOF for the fit to the FIRAS data calibrated at 2.725 K jointed to simulated observations of a spectrum distorted at different cosmic epochs with $\Delta\epsilon/\epsilon_i = 2 \times 10^{-6}$ with a sensitivity of a DIMES-like experiment. We fit 53 data with 2 parameters, T_0 and $\Delta\epsilon/\epsilon_i$, assuming to know the heating epoch.

Figure 37: Values of the fractional energy injected in the radiation field at different epochs as obtained from the fit to the FIRAS data calibrated at 2.725 K jointed to simulated observations of a spectrum distorted at $y_h = 5$ with $\Delta\epsilon/\epsilon_i = 2 \times 10^{-6}$ with a sensitivity of a DIMES-like experiment. The solid line is the best-fit, the dashed lines are the upper and the lower limits at 95% CL. The fit is performed without assumptions on the heating epoch.

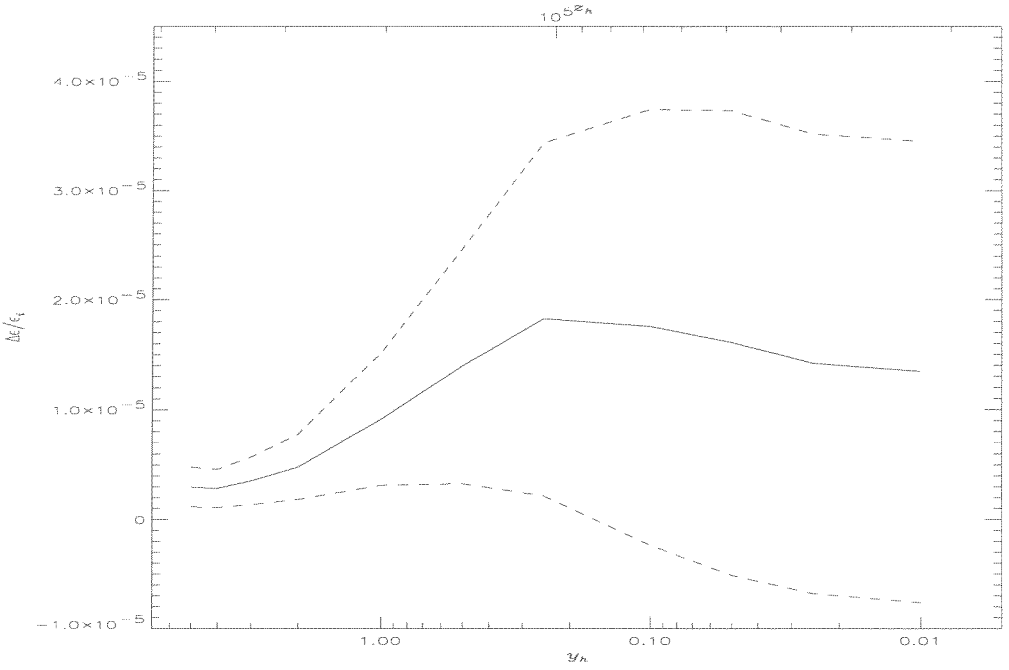

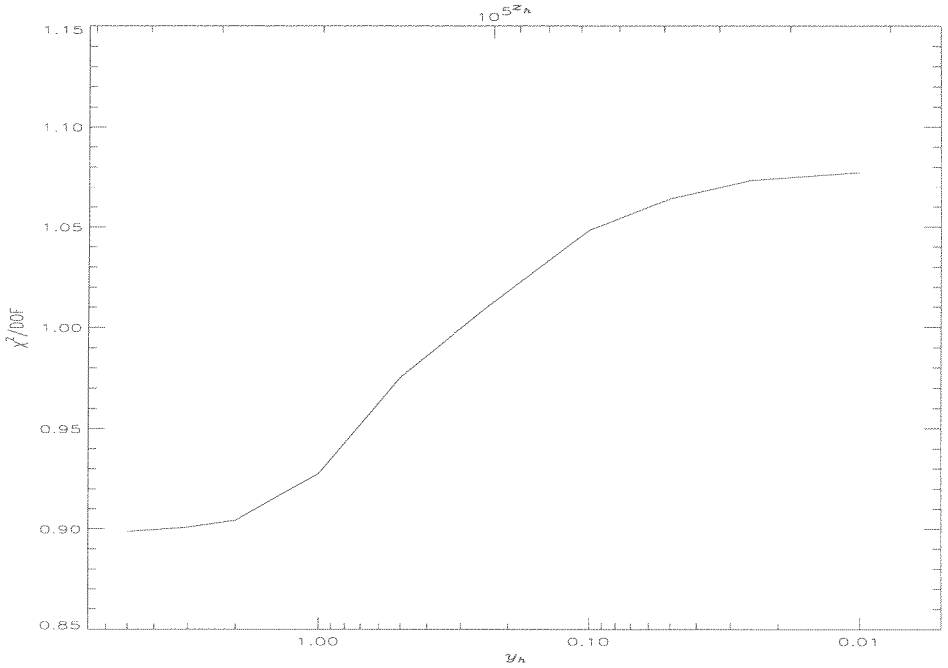

Figure 38: Values of χ^2/DOF for the fit to the FIRAS data calibrated at 2.725 K jointed to simulated observations of a spectrum distorted at $y_h = 5$ with $\Delta\epsilon/\epsilon_i = 2 \times 10^{-6}$ with a sensitivity of a DIMES-like experiment. We fit 53 data with 2 parameters, T_0 and $\Delta\epsilon/\epsilon_i$, without assumptions on the heating epoch.

Figure 39: The same as in Fig. 37 but for a spectrum distorted at $y_h = 1.5$.

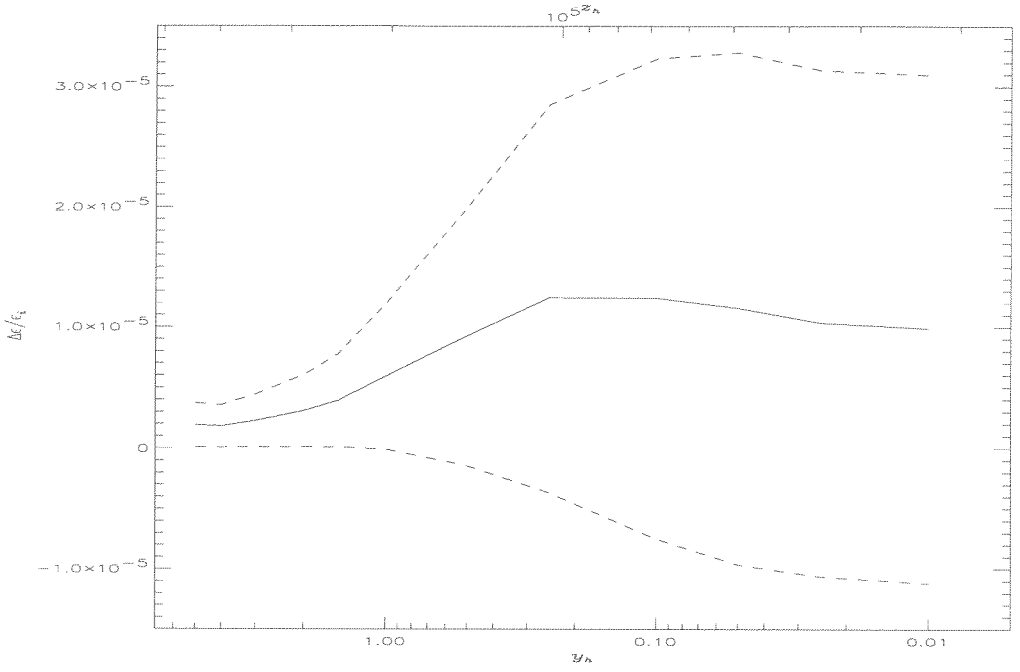

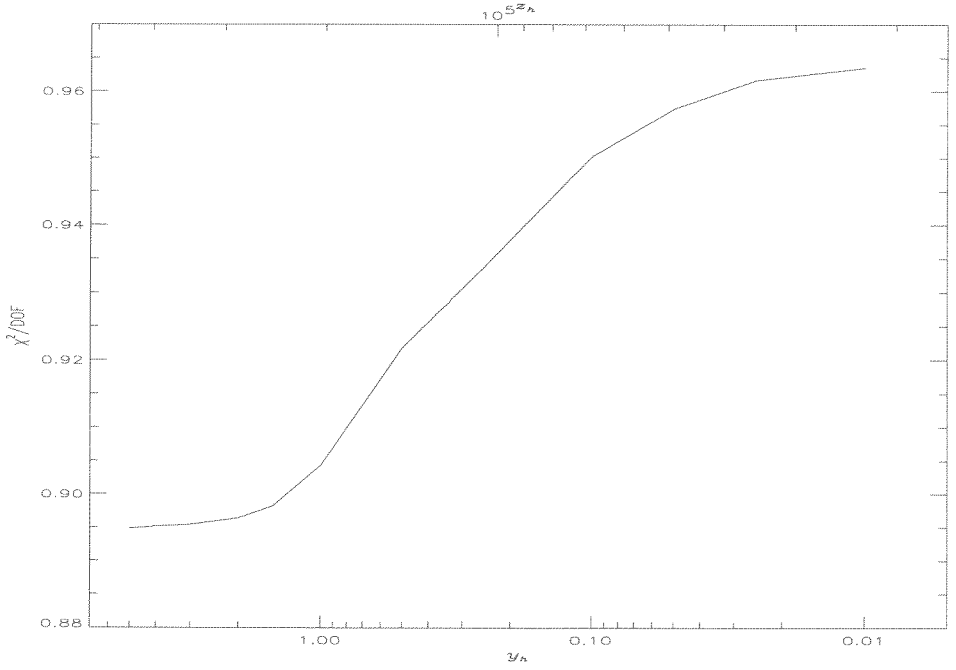

Figure 40: The same as in Fig. 38 but for a spectrum distorted at $y_h = 1.5$.

Figure 41: The same as in Fig. 37 but for a spectrum distorted at $y_h = 0.01$.

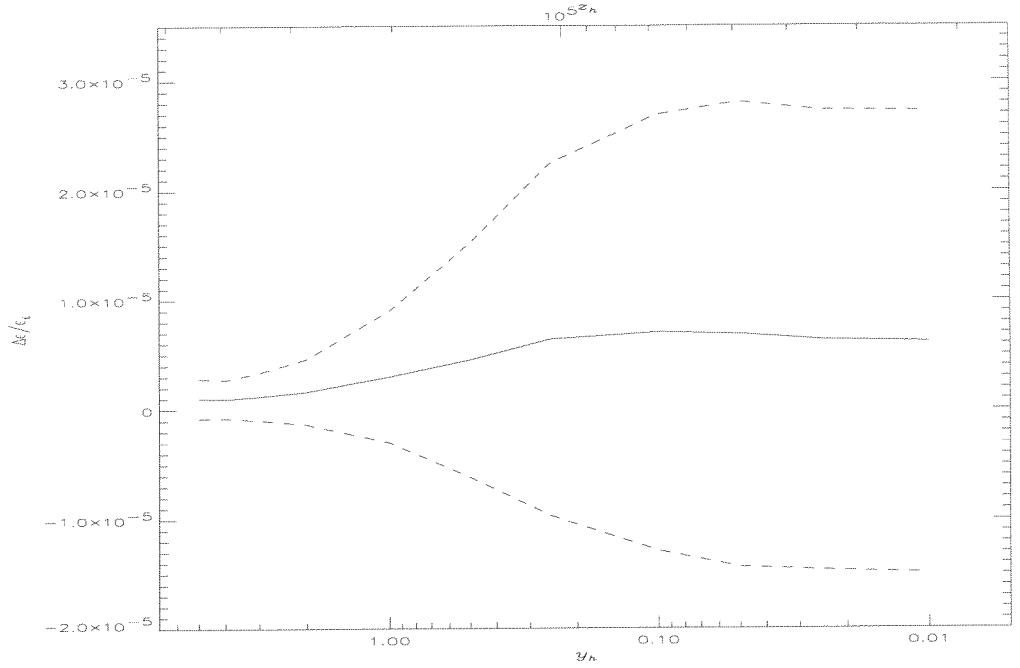

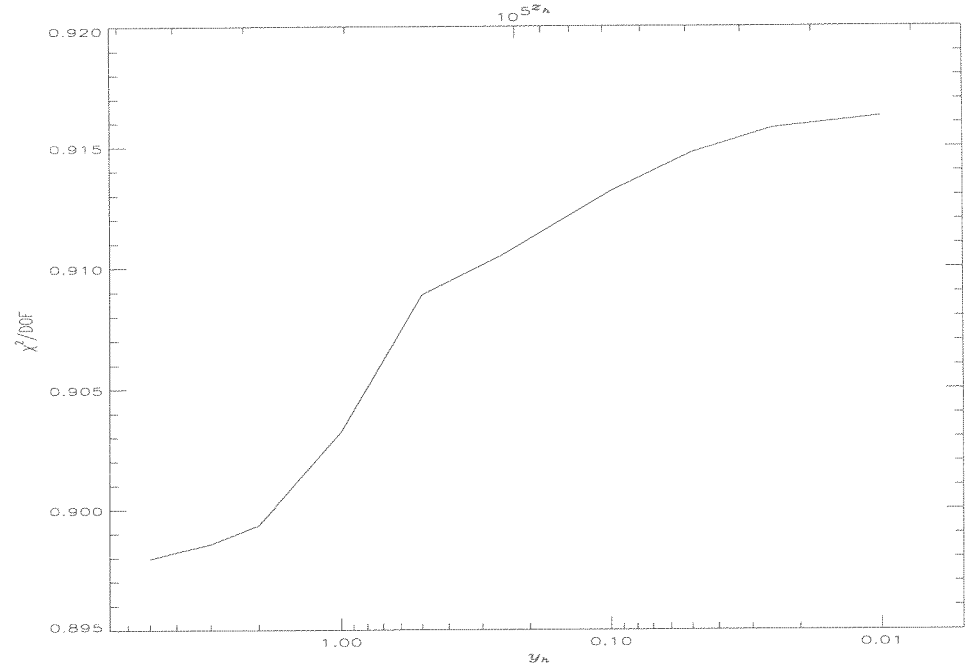

Figure 42: The same as in Fig. 38 but for a spectrum distorted at $y_h = 0.01$.

Figure 43: Values of the fractional energy injected in the radiation field at different epochs as obtained from the fit to the FIRAS data calibrated at 2.725 K jointed to simulated observations of a spectrum distorted at different cosmic epochs with $\Delta\epsilon/\epsilon_i = 2 \times 10^{-4}$ with a sensitivity of a DIMES-like experiment. The solid line is the best-fit, the dashed lines are the upper and the lower limits at 95% CL. The fit is performed assuming to know the heating epoch.

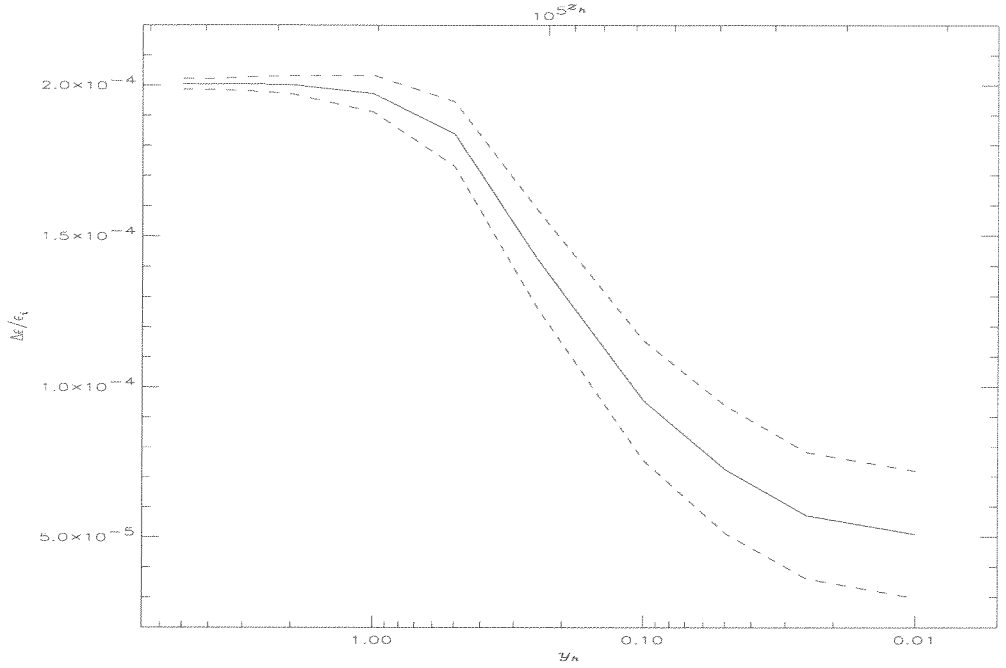

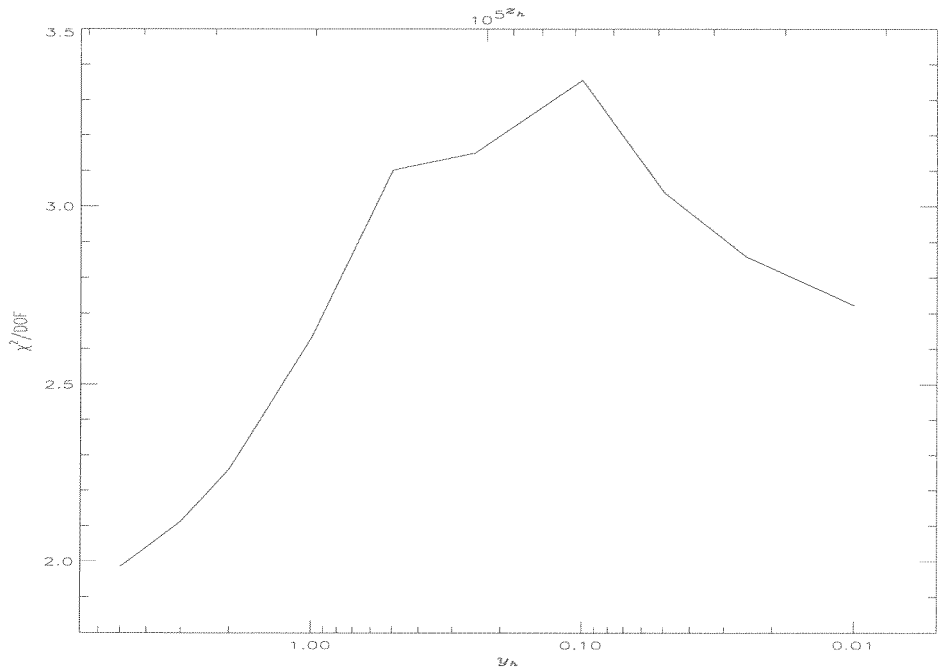

Figure 44: Values of χ^2/DOF for the fit to the FIRAS data calibrated at 2.725 K jointed to simulated observations of a spectrum distorted at different cosmic epochs with $\Delta\epsilon/\epsilon_i = 2 \times 10^{-4}$ with a sensitivity of a DIMES-like experiment. We fit 53 data with 2 parameters, T_0 and $\Delta\epsilon/\epsilon_i$, assuming to know the heating epoch.

References

[1] Battistelli E.S., Fulcoli V., Macculi C. 2000, NA, 5, 77

[2] Burigana C. et al. 1991a, A&A, 246, 59

[3] Burigana C. et al. 1991b, ApJ, 379, 1

[4] Burigana C. et al. 1995, A&A, 303, 323

[5] Burigana C., Salvaterra R. 2000, Int. Rep. ITeSRE/CNR 291/2000

[6] Danese L., Burigana C. 1993, in: "Present and Future of the Cosmic Microwave Background", Lecture in Physics, Vol. 429, eds. J.L. Sanz, E. Martinez-Gonzales, L. Cayon, Springer Verlag, Heidelberg (FRG), p. 28

[7] Danese L., De Zotti G. 1977, Riv. Nuovo Cimento, 7, 277

[8] Fixsen D.J. et al. 1996, ApJ, 473, 576

[9] Kogut A. 1996, astro-ph/9607100

[10] Kompaneets A.S. 1956, Zh. Eksp. Teor. Fiz., 31, 876 [Sov. Phys. JEPT, 4, 730, (1957)]

[11] Mather J.C. et al. 1999, ApJ, 512, 511

[12] Nordberg H.P., Smoot G.F. 1998, Preprint astro-ph/9805123

[13] Pagana E., Villa F., 1996, "The LOBO Satellite Mission: Feasibility Study and Preliminary cost evaluation", Int. Rep. C.I.F.S. - 1996

[14] Press W.H. et al. 1992, "Numerical Recipes in Fortran", second edition, Cambridge University Press, USA

[15] Salvaterra R., Burigana C. 2000, Int. Rep. ITeSRE/CNR 270/2000

[16] Silk J., Stebbins A., 1983, ApJ, 269, 1

[17] Sironi G. et al. 1995, Astro. Lett. Comm., 32, 31

[18] Staggs S. et al. 1996, ApJ, 473, L1

[19] Zeldovich Ya.B., Sunyaev R.A. 1969, Ap&SS, 4, 301

[20] Zeldovich Ya.B., Illarionov A.F., Sunyaev R.A. 1972, Zh. Eksp. Teor. Fiz., 62, 1216 [Sov. Phys. JEPT, 35, 643]